Available online at www.sciencedirect.com

ScienceDirect

Geochimica et Cosmochimica Acta 288 (2020) 83–100

Geochimica et Cosmochimica Acta

www.elsevier.com/locate/gca

Thallium sorption and speciation in soils: Role of micaceous clay minerals and manganese oxides

Silvan Wick [a,b], Bart Baeyens [c], Maria Marques Fernandes [c], Jörg Göttlicher [d], Marlene Fischer [b], Numa Pfenninger [a], Michael Plötze [e], Andreas Voegelin [a,*]

[a] *Eawag, Swiss Federal Institute of Aquatic Science and Technology, Überlandstrasse 133, CH-8600 Dübendorf, Switzerland*
[b] *Institute of Biogeochemistry and Pollutant Dynamics, ETH Zürich, CH-8092 Zürich, Switzerland*
[c] *Paul Scherrer Institute, CH-5232 Villigen PSI, Switzerland*
[d] *Test Facility and Synchrotron Radiation Source, Karlsruhe Institute of Technology, D-76344 Eggenstein-Leopoldshafen, Germany*
[e] *Institute for Geotechnical Engineering, ETH Zürich, CH-8093 Zürich, Switzerland*

Received 5 March 2020; accepted in revised form 27 July 2020; available online 5 August 2020

Abstract

Sorption processes control the solubility of toxic thallium (Tl) in soils and thereby its potential leaching into groundwater or uptake by plants. Micaceous clay minerals and Mn oxides are considered to be key sorbents for Tl in soils. We studied the sorption and speciation of Tl in 36 geogenically Tl-rich topsoil materials from the Swiss Jura Mountains by combining chemical extractions, isotope exchange experiments, adsorption experiments, X-ray absorption spectroscopy (XAS), and sorption modelling. We demonstrate that the relation between exchangeable and soluble Tl determined in batch extractions of soils with only geogenic and with freshly spiked Tl matches adsorption isotherms of freshly spiked Tl, and that this relation can be described with a published 3-site cation exchange model for Tl adsorption onto illite. Complemented with XAS data, the results show that micaceous clay minerals control the short-term solubility of Tl via cation exchange, but also the long-term sequestration of most geogenic soil Tl (>90%) via structural fixation. Adsorption competition with K^+ and NH_4^+ at the frayed edges of micaceous clay minerals greatly affects Tl solubility. Increases in the dissolved concentrations of K and NH_4 in soil pore water may therefore lead to the release of Tl into solution. The fractions of geogenic Tl associated with Mn oxides were about half as high as the fractions of exchangeable Tl. This Mn-associated Tl is not readily mobilized by cation exchange, but could be released during periodic water logging and soil reduction. In (periodically) reducing environments, the potential of Mn oxides for long-term Tl sequestration is therefore limited. In conclusion, the results from this study highlight the importance of micaceous clay minerals for Tl cycling in soils and sediments, and suggest that concepts developed to assess the sorption of (radio)caesium onto micaceous clay minerals in soils and sediments are transferable to Tl.

Keywords: Thallium; Sorption; Soil; Illite; Clay; Minerals; Manganese oxides

1. INTRODUCTION

Thallium (Tl) is a trace metal and a contaminant of substantial concern because it exhibits high toxicity to humans at low dose (Karbowska, 2016; Nriagu, 1998; Peter and Viraraghavan, 2005; Zitko, 1975). Tl concentrations in soils are usually below 1 mg/kg, with an average between 0.2 and 0.5 mg/kg (Kabata-Pendias, 2011; Nriagu, 1998; Tremel et al., 1997b). Geogenic Tl contamination may result from soil formation on mineralized or Tl-enriched parent rock (Bačeva et al., 2014; Tremel et al., 1997b; Vaněk et al., 2009; Voegelin et al., 2015; Xiao et al., 2004). Emissions from metal mining and smelting (Casiot et al., 2011;

* Corresponding author.
E-mail address: andreas.voegelin@eawag.ch (A. Voegelin).

https://doi.org/10.1016/j.gca.2020.07.037
0016-7037/

Vaněk et al., 2011), sulfuric acid production (Chen et al., 2013; Lopez-Arce et al., 2017), coal mining and burning (Cheam et al., 2000; Peter and Viraraghavan, 2005), or cement production (Kersten et al., 2014) may lead to the anthropogenic contamination of soils with Tl. From soils, Tl may leach into groundwater (Karbowska, 2016; Xiao et al., 2003) or enter the food chain (Bunzl et al., 2001; LaCoste et al., 2001; Lehn and Schoer, 1987; Madejón et al., 2007; Makridis and Amberger, 1996; Rader et al., 2019; Tremel et al., 1997a; Vaněk et al., 2010b; Xiao et al., 2004), and may thereby threaten human and environmental health (Tremel et al., 1997a; Xiao et al., 2004; Xiao et al., 2012).

The mobility and bioavailability of Tl in soils is controlled by its speciation and sorption onto soil components. Therefore, qualitative and quantitative information on the speciation of Tl and on key sorption processes is essential to assess risks arising from Tl contaminated soils. In the common pH-Eh range of soils, Tl mainly occurs as relatively well-soluble monovalent Tl(I), and to a lesser extent as highly insoluble trivalent Tl(III) (Nriagu, 1998; Peter and Viraraghavan, 2005). The Tl^+ cation has a similar ionic radius and a similar low hydration enthalpy as the alkali metal cations potassium (K^+), rubidium (Rb^+), and caesium (Cs^+). In analogy to Cs and Rb, Tl can therefore substitute K in minerals such as K-feldspars or replace K in the interlayer of mica (Heinrichs et al., 1980; Jović, 1993; Nriagu, 1998; Shannon, 1976; Wick et al., 2018).

Clay minerals have long been postulated to be key sorbents for Tl(I) in soils and sediments, based on the alkali metal-like behaviour of Tl(I) (Matthews and Riley, 1970; Tremel et al., 1997b). As for Cs and Rb (Cremers et al., 1988; Evans et al., 1983; Sawhney, 1972), especially micaceous clay minerals like illite are commonly assumed to strongly bind Tl in soils (Jacobson et al., 2005a; Nriagu, 1998; Tremel et al., 1997b). This assumption was confirmed in a recent spectroscopic study on geogenically Tl-rich soils (Voegelin et al., 2015), which indicated that Tl in topsoil materials was dominantly Tl(I) associated with illite (or with other micaceous clay minerals). Illite is a non-expandable 2:1 phyllosilicate with a basal spacing of 10 Å and dehydrated K^+ in the collapsed interlayer. In soils, illite is either inherited from sedimentary parent material or formed by the weathering of muscovite (Meunier and Velde, 2004). Weathering involves the release of K at particles edges, resulting in frayed particle edges with an extended basal spacing of 14 Å (Fuller et al., 2015; Jackson, 1968; Meunier and Velde, 2004). At the wedge between the collapsed interlayer and the frayed edges of illite platelets, the alkali metal cations Cs^+ and Rb^+ adsorb with a very high affinity and in competition with K^+, ammonium (NH_4^+), and, to some extent, barium (Ba^{2+}) (Brouwer et al., 1983; Comans et al., 1991; Lee et al., 2017; Meunier and Velde, 2004; Poinssot et al., 1999). The competitive sorption of Cs and Rb onto illite has been successfully modelled using a 3-site cation exchange model (Bradbury and Baeyens, 2000; Poinssot et al., 1999). A low fraction of high-affinity sorption sites (frayed edge sites, FES) and an intermediate fraction of medium-affinity sorption sites (type-2 sites, T2S) account for the specific adsorption of Cs and Rb at the frayed edges of illite platelets, and a large fraction of low-affinity cation exchange sites for non-specific adsorption of Cs and Rb on the planar surfaces of illite (planar sites, PS). In a recent study on the adsorption of Tl onto purified illite, we showed that the adsorption of Tl^+ onto purified Na-, Ca-, K- and NH_4-exchanged illite over wide Tl concentration ranges can be adequately described with the 3-site cation exchange model (Wick et al., 2018). The corresponding cation exchange selectivitiy coefficients showed that Tl adsorbs very strongly onto illite (as confirmed in another recent sorption study (Martin et al., 2018)), with an adsorption affinity between the affinities of Cs and Rb. X-ray absorption near edge structure (XANES) spectra indicated that FES and T2S model sites served to describe the adsorption of (dehydrated) Tl at illite particle edges (Wick et al., 2018). The parameterized cation exchange model allows describing the adsorption of Tl onto purified illite in the presence of competing cations. To date, however, the ability of this model to predict the adsorption of Tl onto illite or, more generally, onto micaceous clay minerals in soils has not been evaluated.

Manganese (Mn) oxides can accumulate high levels of Tl in marine and terrestrial deposits (Crittenden et al., 1962; Koschinsky and Hein, 2003; Nriagu, 1998; Peacock and Moon, 2012; Rehkämper et al., 2004; Rehkämper and Nielsen, 2004), and may also be important for Tl retention in soils (Tremel et al., 1997b; Vaněk et al., 2011; Voegelin et al., 2015). In soils, Mn oxides form by microbial or autocatalytic oxidation of Mn^{2+} (Gilkes and McKenzie, 1988; Tebo et al., 2004) and can occur as local accumulations referred to as Mn-concretions (Blume et al., 2016). Strong Tl sorption by Mn oxides has been attributed to three uptake mechanisms: (i) Oxidation of Tl(I) and complexation of Tl(III) by vacancy-containing birnessite (Cruz-Hernández et al., 2019; Peacock and Moon, 2012; Wick et al., 2019), (ii) sorption of hydrated Tl(I) by, e.g., triclinic birnessite or todorokite (Peacock and Moon, 2012; Wick et al., 2019), or (iii) structural incorporation of dehydrated Tl^+, for example in cryptomelane (Crittenden et al., 1962; Wick et al., 2019). Laboratory sorption experiments have shown that oxidative Tl scavenging by vacancy-containing δ-Mn(IV)O_2, a synthetic analogue of biogenic Mn oxides (Post, 1999; Tebo et al., 2004), can lead to very high Tl loadings at very low dissolved Tl concentrations (Wick et al., 2019). The partial reduction and structural transformation of fresh δ-MnO_2 inhibits further oxidative Tl uptake (Wick et al., 2019). Nevertheless, partly-reduced and/or transformed δ-MnO_2, as well as triclinic birnessite, todorokite, and cryptomelane also exhibit a high sorption affinity for Tl(I) relative to illite (Wick et al., 2019). Birnessite additions to Tl-containing soil have been shown to effectively reduce Tl uptake by white mustard (Vaněk et al., 2011), and significant fractions of soil Tl were observed to be extractable in the reductive step of sequential extractions supposed to dissolve Mn oxides (Antić-Mladenović et al., 2017; Gomez-Gonzalez et al., 2015; Vaněk et al., 2009; Vaněk et al., 2011; Yang et al., 2005). These results thus point to the relevance of Mn oxides for

Tl retention in soils. In a spectroscopic study on geogenically Tl-rich soils, Tl(III) associated with soil Mn concretions was identified by point analyses. Bulk analyses on corresponding topsoil samples, on the other hand, indicated that most geogenic Tl was Tl(I) associated with micaceous clay minerals (Voegelin et al., 2015). Factors that can limit the relevance of Mn oxides for Tl retention in soils include their usually low abundance relative to micaceous clay minerals, their susceptibility to reductive transformation or dissolution (Wick et al., 2019), and strong sorption competition with other major and trace metal cations (Wick et al., 2019). To date, the importance of Mn oxides for Tl retention in soils still remains uncertain.

The aim of the present study is to gain new insights into the relevance of micaceous clay minerals and Mn oxides for Tl sorption in soils and a better understanding of their impacts on dissolved Tl concentrations. We therefore studied the sorption and speciation of Tl in geogenically Tl-rich topsoils formed on mineralized dolomitic rocks in the Swiss Jura mountains (Herrmann et al., 2018; Truninger, 1922; Voegelin et al., 2015). We used XANES spectroscopy to characterize Tl speciation, chemical extractions and isotopic exchange to quantify the pool of exchangeable Tl, and sequential extractions to estimate the fraction of Tl associated with Mn oxides. The relationship between exchangeable and soluble Tl in geogenically Tl-rich soils and adsorption isotherms determined on freshly Tl-spiked soils were predicted and interpreted using the cation exchange model for Tl sorption onto illite (Wick et al., 2018) and sorption isotherms for Tl sorption onto Mn oxides (Wick et al., 2019).

2. MATERIALS AND METHODS

2.1. Sampling site

The locality Erzmatt (“ore meadow”) is a meadow near the village of Buus in the Swiss Jura Mountains (47° 30′20″N, 7°51′07″E). The soils on the Erzmatt show high levels of Tl, arsenic (As), and iron (Fe) of geogenic origin (Truninger, 1922; Voegelin et al., 2015). The soil parent material at the site consists of dolomitized sediments (Stamberg member (former name: Trigonodus dolomite), Ladinian as a part of the Schinznach formation (former name Upper Muschelkalk), Triassic) (Adams and Diamond, 2019; Pietsch et al., 2016; Schauer and Aigner, 1997) that are locally mineralized (Truninger, 1922). This hydrothermal Tl-As-Fe mineralization is most probably linked to Upper Rhine Graben tectonics (Gonzalez, 1990) that triggered uprising fluids during Oligocene and Miocene time. Still active hot springs in the northern Upper Rhine Graben (Germany) may be considered as a recent analogue of such hydrothermal systems (Loges et al., 2012). The observation of Tl- and As-bearing jarosite and avicennite in soil samples from the Erzmatt suggest that the unweathered ore body consisted of Tl-As-Fe sulfides (Herrmann et al., 2018; Truninger, 1922; Voegelin et al., 2015). The Erzmatt was not covered by ice during the last glacial maximum, suggesting that soils at the site may be more than 10,000 years old. The soils belong to the Cambisol group, exhibit weak redoximorphic features and have a neutral to slightly acidic pH (Fig. S1). The climate in the area is temperate (mean annual air temperature approx. 9 °C; mean annual precipitation approx. 960 mm) (Voegelin et al., 2015).

2.2. Soil sampling

For the present study, topsoil samples from the Erzmatt were kindly provided by the cantonal authorities (Amt für Umwelt und Energie (AUE), Kanton Basel-Landschaft), which performed an extensive monitoring campaign between 2012 and 2014 to determine the extension of the geochemical anomaly on the Erzmatt. At about 150 sites, four topsoil cores (0–20 cm depth) were taken, pooled, and air-dried at 40 °C. The pooled samples were sieved to 2 mm and stored in polyethylene (PE) containers. Based on acid-extractable element contents and soil pH values determined by the cantonal authorities, 36 topsoil samples were selected for this study. These samples cover geogenic Tl contents from ~3 to ~1000 mg/kg and also vary with respect to Mn, Fe, calcium (Ca), and magnesium (Mg) contents as well as pH values. Based on acid-extractable Tl contents, the 36 topsoil samples were arranged in six groups of six samples each (A1-A6 with ~3 mg/kg, B1-B6 with ~10 mg/kg, C1-C6 with ~30 mg/kg, D1-D6 with ~100 mg/kg, E1-E6 with ~300 mg/kg, and F1-F6 with ~1000 mg/kg Tl).

A topsoil sample from an earlier study on the Erzmatt (P1 00-20; 100 mg/kg Tl (Voegelin et al., 2015)) was used to extract the clay mineral fraction. First organic matter was decomposed (hydrogen peroxide, 80 °C), followed by the removal of Fe and Mn oxides (dithionite, 80 °C). After sodium (Na) exchange followed by dialysis, the clay fraction was separated by centrifugation. Subsequently, the clay minerals were flocculated with Na, concentrated by settling, and stored as suspension in the dark at 4 °C.

2.3. Bulk soil analyses

Total element contents were determined using an energy-dispersive X-ray fluorescence spectrometer (XRF; Xepos+, SPECTRO Analytical Instruments GmbH, Germany) with a built-in calibration for geological samples. For XRF analysis, 4.0 g of soil material was ground in a ball mill, mixed with wax and pressed into a 32-mm diameter pellet. Total contents of carbon (C) and nitrogen (N) (CNS total element analyser, EuroVector) and the contents of inorganic C (Coulomat, UIC, Inc.) were measured, and the contents of organic C calculated as the difference between total and inorganic C contents. Soil texture was measured using a laser diffraction grain sizer (Hydro 2000S, Mastersizer 2000, Malvern Instruments Ltd, U. K.), after overnight dispersion of the soils in 0.1% calgon solution.

The mineralogy of six soil samples with different total Tl loadings (A6, B4, C5, D1, D6, E6) was determined on randomly oriented powder samples by X-ray diffraction (XRD) analysis (details in the Appendix). Samples were

ground (<20 μm) and filled into frontloading sample holders. X-ray diffraction patterns were measured with a Bragg-Brentano diffractometer (BRUKER AXS D8) using Co K_α radiation. The qualitative phase composition was determined with the software DIFFRAC.EVA (BRUKER AXS) and the quantitative determination of the mineralogical composition was carried out by Rietveld analysis using the Rietveld program Profex/BGMN (Bergmann et al., 1998; Bergmann and Kleeberg, 1998; Döbelin and Kleeberg, 2015; Omotoso et al., 2006).

2.4. Exchangeable cations

All soils were extracted with 1 M NH_4-acetate (pH 6.8) to quantify the pools of exchangeable cations. For the extraction, 1.5 g of soil were weighed into 50 mL PE tubes and extracted in two consecutive steps with 12.5 mL 1 M NH_4-acetate each (2 × 30 min; horizontal table shaker; 350 rpm). After each step, the samples were centrifuged (5 min; 2700 *g*) and 10 mL of supernatant filtered (0.2 or 0.45 μm nylon membranes). Subsequently, the two filtered extracts were pooled and acidified (65% HNO_3, 1% v/v). The combined extracts were diluted with 1% HNO_3 and analysed for Mg, K, Ba, Ca, Mn, Rb, Tl, and further elements using an inductively coupled plasma mass spectrometer (ICP-MS; Agilent 7500ce or Agilent Triple Quadrupole 8900). For each soil, the extraction was performed at least in duplicates and the determined amounts of exchangeable cations were averaged. To assess the completeness of the two-step extraction, six soil samples (A5, B2, C3, D5, E5, F5) were also extracted in four consecutive steps and the extracts from each step were analysed by ICP-MS individually. To determine exchangeable NH_4^+, 1.0 g of the soil materials was extracted in 5 mL of 2 M KCl for 30 min on a table shaker (350 rpm). After reaction, the suspensions were centrifuged and filtered (0.2 μm nylon membranes) and the filtrates analysed for NH_4^+ using colorimetric photometry (indophenol blue method; Cary 50-3 photometer, or Hach-Lange cuvette test (LCK304)).

2.5. Pseudo-porewater extracts

All soils were extracted with 0.01 M Ca-chloride ($CaCl_2$) to determine the soil pH value and dissolved cation concentrations in pseudo-porewater (Houba et al., 2000). In 50 mL PE tubes, 2.0 g of soil were extracted with 20 mL of $CaCl_2$ (solid-to-solution ratio 0.1 kg/L) for 2 h (horizontal table shaker; 350 rpm). After extraction and centrifugation (5 min; 2700 *g*), 10 mL of the supernatant were filtered (0.2 or 0.45 μm nylon membranes) and acidified (65% HNO_3, 1% v/v). The pH value was measured in the remaining re-suspended extract. The samples were diluted with 1% HNO_3 and analysed for Na, K, Ba, Mg, Ca, Mn, Rb, Tl, and further elements using ICP-MS. NH_4^+ was determined by colorimetric photometry (Cary-50-3 and LCK304). Each soil was extracted at least in duplicates and cation concentrations were averaged. A subset of samples (A5, B2, C3, D5, E5, F5) was equilibrated with 0.01 M $CaCl_2$ four times in sequence to assess changes in dissolved Tl over multiple equilibrations.

2.6. Solid-liquid distribution coefficients for exchangeable geogenic Tl

Solid-liquid distribution coefficients for exchangeable geogenic Tl ($^{Tl}K_{d,geo}$, in [L/kg]) were calculated according to Eq. (1):

$$^{Tl}K_{d,geo} = \frac{Q_{Tl,NH_4}}{C_{Tl,Ca}} \quad (1)$$

$Q_{Tl,NH4}$ corresponds to the amount of Tl exchanged with NH_4-acetate (in [mol/kg]) and $C_{Tl,Ca}$ to the concentration of Tl in the $CaCl_2$ pseudo-porewater extracts (in [mol/L]). Distribution coefficients for other cations (K, Rb, Ba, Mg) were calculated analogously. From the distribution coefficients of monovalent Tl, Rb and K, cation exchange selectivity coefficients were calculated as follows (e.g. for Tl-Rb exchange in Eq. (2)):

$$^{Tl,Rb}K_{ex,geo} = \frac{^{Tl}K_{d,geo}}{^{Rb}K_{d,geo}} \quad (2)$$

2.7. Isotope exchange experiment

With six selected soils (A6, B4, C5, D1, D6, E6), a kinetic isotope exchange experiment with radioactive ^{204}Tl was performed in 0.01 M $CaCl_2$ electrolyte to estimate independently the pool of (exchangeable) Tl that interacts with the solution. For this purpose, 1.0 g of dried soil was suspended in 10 mL 0.01 M $CaCl_2$ in 40 mL polypropylene centrifuge tubes (Beckman Coulter). After 2 h of equilibration, ^{204}Tl was spiked to the suspensions (total ~9×10^{-12} mol Tl added with a ^{204}Tl activity of ~660 Bq; more information on the ^{204}Tl tracer is given in Wick et al., 2018). The samples were subsequently reacted for 4 h and 1, 3, 7, 14, 30, and 90 days (d). For sampling, the suspensions were centrifuged (5 min, 2700 *g*) and 2 mL of the supernatant were diluted with 3 mL 0.01 M $CaCl_2$ and 15 mL scintillation cocktail (UltimaGold X/R, Merck). Solution pH was measured in the remaining supernatant. The ^{204}Tl activity was analysed using a liquid scintillation counter (Packard Tri-Carb 2750 TRILL). From the decrease in the ^{204}Tl activity, the distribution coefficients $^{Tl\text{-}204}K_d$ (in [L/kg]) were calculated according to Eq. (3):

$$^{Tl-204}K_d = \frac{Q}{C} = \frac{(C_{Tl-204,init.} - C_{Tl-204,final})}{C_{Tl-204,final}} \times \frac{V}{m} \quad (3)$$

$C_{Tl\text{-}204,init}$ and $C_{Tl\text{-}204,final}$ are the initial and final ^{204}Tl activity in solution, respectively, V the solution volume (in [L]) and m the mass of soil (in [kg]). Each experiment was run in duplicates, and the resulting $^{Tl\text{-}204}K_d$ values were averaged.

In parallel to the experiment with radioactive ^{204}Tl, the same experiment was also performed without ^{204}Tl tracer spike. Solutions from this inactive experiment were filtered, acidified and analysed for Na, Mg, K, Ca, Rb, and Tl using ICP-MS and photometrically (Cary 50-3) for NH_4. The experiment was performed in duplicates and measured concentrations were averaged. From Tl concentrations measured in the inactive samples ($C_{Tl,Ca}(t)$, in [mol/L]) and the distributions coefficients of ^{204}Tl ($^{Tl\text{-}204}K_d(t)$, in

[L/kg]) after equilibration time t, the pools of radiolabile soil Tl ($E_{Tl}(t)$, in [mol/kg]) were calculated using Eq. (4):

$$E_{Tl}(t) = {}^{Tl-204}K_d(t) \times C_{Tl,Ca}(t) \quad (4)$$

2.8. Sequential soil extraction

18 soil samples (A1, A2, A6, B1, B2, B6, C1, C2, C6, D1, D2, D6, E1, E2, E6, F1, F2, and F6) were extracted in a two-step sequential extraction to quantify the pools of exchangeable cations and Tl associated with Mn oxides. For the extraction, 1.0 g of soil was weighed into a dark 50 mL polypropylene tube. In the first step, the soils were extracted three times with 30 mL 1 M NH_4-acetate (pH 6.8) for 30 min. In the second step, the soils were extracted three times with 30 mL of 0.1 M hydroxylamine hydrochloride ($NH_3OH \times HCl$) and 1 M NH_4-acetate (pH 6.1) (adapted from Zeien and Brümmer (1989)) for 30 min. In both steps, the individual extracts were collected by centrifugation, filtered, acidified and diluted as required for analysis by ICP-MS.

2.9. Tl adsorption / re-extraction experiments

Six soil samples (A6, B4, C5, D1, D6, and E6) with geogenic Tl contents of ~3 to ~350 mg/kg were selected for Tl adsorption / re-extraction experiments. The adsorption and re-extraction experiments were performed three times with subsets of soils, using nearly the same protocol with minor variations (see Appendix for details). In general, 2.0 g of dried soil were weighed into 50 mL polypropylene tubes and conditioned two times with 20 mL 0.01 M $Ca(NO_3)_2 \times 4H_2O$ / 0.0001 M KNO_3 solution for 2 h, recording the pH and measuring element concentrations in the conditioning solutions. For Tl adsorption, 0.01 M $Ca(NO_3)_2$ solutions were spiked with seven Tl concentrations (from $\sim 3.5 \times 10^{-7}$ to $\sim 4.5 \times 10^{-4}$ M) using 0.01 M or 0.001 M $TlNO_3$ (Sigma Aldrich) stock solutions. The wet soil materials (2.0 g of soil and ~1.6 g conditioning solution) were then suspended in 20 mL of the Tl-containing electrolyte solutions and reacted for seven days on a table shaker (350 rpm) at room temperature. After reaction, the suspensions were centrifuged and the supernatant filtered (0.2 µm nylon membrane) and acidified (1% v/v HNO_3 suprapur) for the analysis of Na, Mg, K, Ca, Rb, Ba and Tl using ICP-MS. The solution pH was recorded in the suspensions after solution sampling and resuspension. The residual wet soil was kept in the fridge in the dark. The difference between spiked and residual dissolved Tl was assumed to correspond to Tl adsorbed to the soil. The total amount of adsorbed Tl was calculated by adding the amounts of NH_4-exchangeable geogenic Tl in the individual soils prior to Tl adsorption to the amounts of freshly sorbed Tl (based on NH_4-acetate extraction of soils from sorption experiments without Tl spike).

After Tl adsorption, the reacted soils were first extracted with 20 mL 0.01 M $CaCl_2$ to determine pseudo-porewater concentrations (as described above for geogenic Tl). In a second step, the soils were extracted twice with 20 mL 1 M NH_4-acetate to determine the amounts of NH_4-exchangeable Tl (as described above for geogenic Tl). After sorption and between the two extraction steps, supernatants were decanted as completely as possible and the wet soils were stored at 4 °C in the dark. Carryover of Tl or other elements from residual solution into the next extraction step and dilution of the extracts by residual solution was calculated from solution composition and the gravimetrically determined volume of residual solution.

2.10. X-ray adsorption near edge structure spectroscopy

The speciation of geogenic Tl in 16 topsoil samples (B4, B5, B6, C1, C4, C5, C6, D1, D5, D6, E5, E6, F3, F4, F5, and F6) with total Tl contents from ~10 to ~1000 mg/kg Tl and in one topsoil clay mineral fraction (P1 00-20 clay) and of freshly adsorbed Tl in three topsoil samples (A6 with 100 mg/kg and 1000 mg/kg spiked Tl, D1 with 1000 mg/kg spiked Tl) was characterized using Tl L_{III}-edge (12,658 eV) XANES spectroscopy. The dried samples were ground with an agate mortar and pestle, mixed with cellulose and pressed into 7-mm diameter pellets for analysis. The samples were measured at room temperature in fluorescence mode at the SuperXAS beamline (Swiss Light Source (SLS), Switzerland), the SUL-X beamline (Synchrotron Radiation Source at Karlsruhe Institute of Technology, Germany) and the Dutch-Belgian Beamline (DUBBLE) (European Synchrotron Radiation Facility (ESRF), France).

Data extraction and normalization were performed with Athena (Ravel and Newville, 2005). A linear curve fit to the pre-edge region (−100 to −30 eV relative to E_0 set to 12,668 eV) was subtracted for background removal and a cubic function fit to the post-edge region (+40 to +280 eV relative to E_0) was used to normalize the edge step to unity (at E_0) and to flatten the post-edge region. Analysis of the normalized XANES spectra over the energy range 12,648–12,768 eV by linear combination fitting (LCF) was performed with software from beamline 10.3.2 at the Advance Light Source (Berkeley, USA) (Marcus et al., 2004). Out of a larger set of reference spectra (Fig. S4), four reference spectra were selected for LCF analysis, as further detailed in the Appendix: (i) Tl(I)-illite (illite with Tl loading of 3800 mg/kg Tl from Wick et al. (2018)), representing dehydrated Tl^+ adsorbed at the frayed edges of illite or other micaceous clay minerals, (ii) Tl(I)-muscovite (Ba-rich muscovite ("oellacherite") from Lengenbach (Switzerland) with ~200 mg/kg Tl(I)), representing structural Tl in the interlayer of micaceous clay minerals, (iii) dissolved aqueous Tl^+ (0.01 M $TlNO_3$) as proxy for (hydrated) Tl^+ adsorbed onto clay minerals (Wick et al., 2018), Mn oxides such as triclinic birnessite or todorokite (Wick et al., 2019), soil organic matter or Fe oxides and (iv) Tl(III) sorbed onto δ-MnO_2 (spectrum Na-δ-MnO_2 with 0.021 Tl/Mn from Wick et al. (2019)) as proxy for Tl(III) sorbed onto Mn oxides (or in Tl_2O_3). Starting with the best one-component fit, the number of fit components was increased as long as the normalized sum of the squared residuals ($NSSR = \sum(data_i - fit_i)^2 / \sum data_i^2$) of the best fit decreased by at least 20%.

2.11. Modelling of Tl adsorption onto micaceous clay minerals

The adsorption of Tl onto micaceous clay minerals was predicted for geogenic Tl in all studied soils as well as for freshly adsorbed Tl on the six soils used for the adsorption experiment. The 3-site cation exchange model for the adsorption of Tl, Rb, NH_4, K, Na, and Ca onto illite (Wick et al., 2018) was implemented in the geochemical equilibrium code PhreeqC (Parkhurst and Appelo, 1999). For Mg, the same cation exchange coefficients as for Ca were assumed. For the solution speciation, the database Minteq V4 was used. For Tl(I), free Tl^+ and the complexes $TlNO_3$, TlCl and $TlCl_2^-$ were taken into account. Oxidation of Tl(I) to Tl(III) and precipitation of Tl(I)-phases were excluded in the calculations.

For geogenic Tl, a first calculation was run for different dissolved Tl concentrations in the $CaCl_2$ extracts, but at constant concentrations of Rb, NH_4, K, Na, Mg, and Ca corresponding to the average (or the 5-percentile or 95-percentile) of their concentrations in the $CaCl_2$ extracts from all soils. The cation concentrations were charge-balanced with nitrate (NO_3^-). Comparison of model calculations with Cl^- instead of NO_3^- as charge-balancing anion showed that results for free Tl^+ and sorbed Tl(I) varied by less than 2%; reflecting the fact that neither nitrate nor chloride form strong complexes with Tl^+ or the other modelled cations. The modelled cation loadings on illite were scaled by assuming an average content of illite and mica (dioctahedral micaceous phyllosilicates) of 16.8% for all soils (details in the Appendix). A second calculation for geogenic Tl was run with the individual pseudo-porewater cation concentrations for each soil charge-balanced by NO_3^-. The resulting cation loadings on illite were either scaled by the same average clay content, or by the clay content of each soil individually (details in the Appendix). For the calculation of the adsorption isotherms for the soils A6, B4, C5, D1, D6, and E6, the concentrations of Rb, NH_4, K, Na, Mg, and Ca were derived from the individual pseudo-porewater extracts, and the clay content was set to the fraction of mica and illite determined by XRD analysis (details in the Appendix).

2.12. Tl sorption onto Mn/Fe-enriched and depleted soil material from an acidic pseudogley soil

To gain further insights into the Tl adsorption behaviour in soils and the potential role of Mn oxides therein, Tl adsorption experiments were also performed with Mn/Fe-enriched and Mn/Fe-depleted soil material from an acidic pseudogley soil (stagnosol group), in analogy to the sorption experiment with soils from the Erzmatt described above. Tl L_{III}-edge XANES spectra of the Tl-sorbed soil materials were collected at the SAMBA beamline (Synchrotron Soleil, Gif-sur-Yvette, France). Details on the soil material (characterization) and on the Tl adsorption experiment are given in the Appendix.

3. RESULTS

3.1. Physicochemical soil characterization

In Table 1, selected physicochemical properties are listed for the six soil materials used for Tl adsorption re-extraction experiments (A6, B4, C5, D1, D6, and E6) together with the average and range for all 36 topsoil samples. The complete characterization results are given in Tables S1-S3. The soil samples had a pH_{CaCl2} between 5.0 and 7.6, and contained between 1.0% and 8.4% organic C. Their Fe content ranged between ~8000 and ~72,000 mg/kg and their Mn content between ~260 and ~1700 mg/kg. The mineralogical analysis of the six samples used in the adsorption / re-extraction and isotope exchange experiments (Table S2) indicated that phyllosilicates (chlorite, illite, kaolinite, muscovite) accounted for 20–29% of the soil mass, and that micaceous clay minerals (illite and

Table 1
Soil pH, organic and inorganic C content, clay size fraction, XRD results (illite, muscovite, sum of phyllosilicates), total Mn and Tl (XRF) and extractable element contents for the six soil samples used in the adsorption / re-extraction and isotope exchange experiments and the corresponding average values, standard deviations and ranges for all analyzed soil samples.

	Selected individual soils						All analyzed soils[a]	
	A6	B4	C5	D1	D6	E6	Average	Range
pH_{CaCl2}	6.9	7.2	7.1	7.0	6.6	7.2	6.8 (0.6)	5.0–7.6
Organic C (wt%)	3.1	2.9	5.0	3.1	2.6	5.2	3.9 (1.3)	1.0–8.4
Inorganic C (wt%)	0.2	2.0	3.2	0.2	0.1	2.0	1.6 (2.5)	0.0–11
Clay size fraction (wt%)	11.1	8.8	5.5	15.1	17.4	7.7	11 (4.1)	5.5–20
Illite (wt%)	9.2	10.4	10.3	11.3	12.2	11.8	11 (1.0)	–
Muscovite (wt%)	8.1	5.2	3.5	8.6	5.8	4.1	5.9 (1.9)	–
Illite + muscovite (wt%)	17.3	15.6	13.8	19.9	18.0	15.9	16.8 (2.0)	–
All phyllosilicates (wt%)	25.9	21.6	17.5	28.9	26.3	19.6	23.3 (4.0)	–
Mn_{tot} (mg/kg)	1190	1070	910	1330	1240	1090	1050 (290)	260–1680
Tl_{tot} (mg/kg)	3.1	7.6	27	73	100	350	203 (289)	2.2–1030
Tl_{NH4} (mg/kg)	0.1	0.3	0.6	2.3	3.2	16	9.7 (16)	0.05–54
Tl_{CaCl2} (μg/L)	0.2	0.6	2.0	5.1	4.9	50	30 (50)	0.1–270

[a] Average with standard deviation in parenthesis and range for all 36 analyzed soil samples, except for XRD results, where the averages and standard deviations for the six soil samples A6, B4, C5, D1, D6, and E6 are listed.

muscovite) represented the dominant phyllosilicate fraction (16–20%). The non-clay fraction was dominated by quartz (32–42%), K-feldspar (11–26%), and variable proportions of dolomite.

The total Tl concentration in the soil samples ranged from 2.2 to 1030 mg/kg (Table S3). The correlation analysis of total element contents (Table S4) revealed a very close correlation between Tl and As ($r = 0.99$) confirming their common origin from a hydrothermal Tl-As-Fe-sulfide mineralization, which was also reflected in the correlation of Tl (and As) with Fe ($r = 0.78$), and Sr ($r = 0.75$). The correlation between Ca and Mg ($r = 0.86$) pointed to dolomite as the major Ca and Mg source. Finally, the correlations of Al with Si ($r = 0.96$), K (0.87), Ba (0.88), and Rb (0.93) was attributed to the presence of these elements in primary silicates (quartz, feldspar) and phyllosilicates inherited from the soil parent material.

3.2. Exchangeable cations

Exchangeable Tl determined by the two-step 1 M NH_4-acetate extraction ranged from 0.05 to 55 mg/kg (Table 1). The complete extraction results are given in Table S5. Exchangeable Tl closely correlated with total soil Tl ($r = 0.98$ for log-transformed Tl contents; Fig. 1A), and on average $3.6 \pm 1.6\%$ of the total soil Tl were exchangeable. Regression analysis indicated that the fraction of exchangeable Tl slightly decreased with increasing pH ($(Tl_{NH4}/Tl_{tot}) = (12.5–1.32 \times pH_{CaCl2})\%$). Averaged over all soils, exchangeable Ca accounted for $78 \pm 9\%$, Mg for

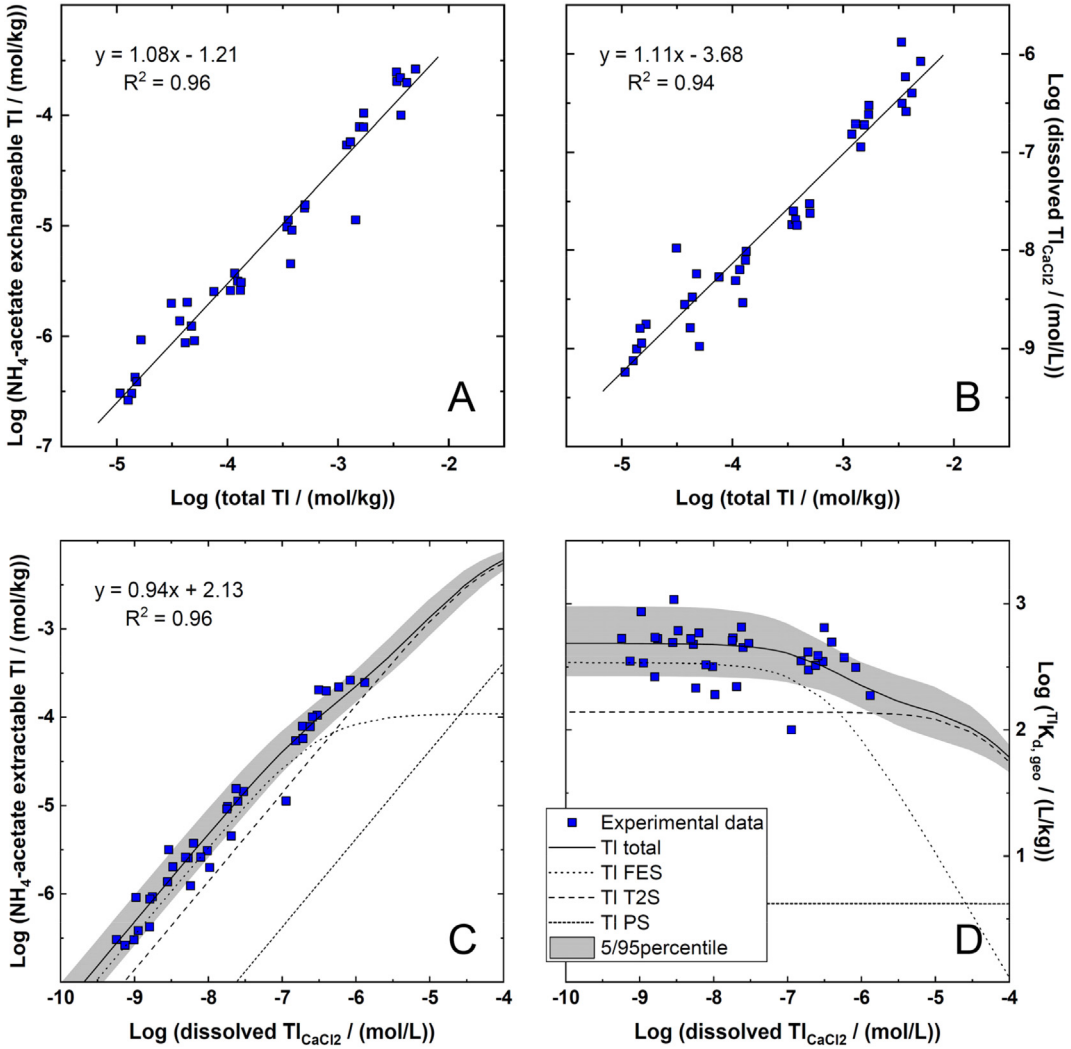

Fig. 1. (A) Exchangeable Tl (1 M NH_4-acetate) and (B) dissolved Tl in pseudo-porewater extracts (0.01 M $CaCl_2$) versus total soil Tl contents, including linear regressions. (C) Exchangeable versus dissolved Tl as pseudo-isotherm for geogenic soil Tl, with linear regression parameters (line not shown). (D) Corresponding plot of the log transformed distribution coefficients $^{Tl}K_{d,geo}$ versus dissolved Tl concentrations. Lines in panels (C) and (D) represent predictions based on the 3-site cation exchange model for Tl(I) adsorption onto illite (Wick et al., 2018) (total, frayed edge sites (FES), type-2 sites (T2S), planar sites (PS)) for average dissolved concentrations of Rb, NH_4, K, Mg, and Ca in pseudo-porewater extracts scaled for a micaceous soil clay mineral content (illite and muscovite) of 16.8%. The grey area is limited by model predictions for 5-percentile and 95-percentile cation concentrations in the pseudo-porewater extracts.

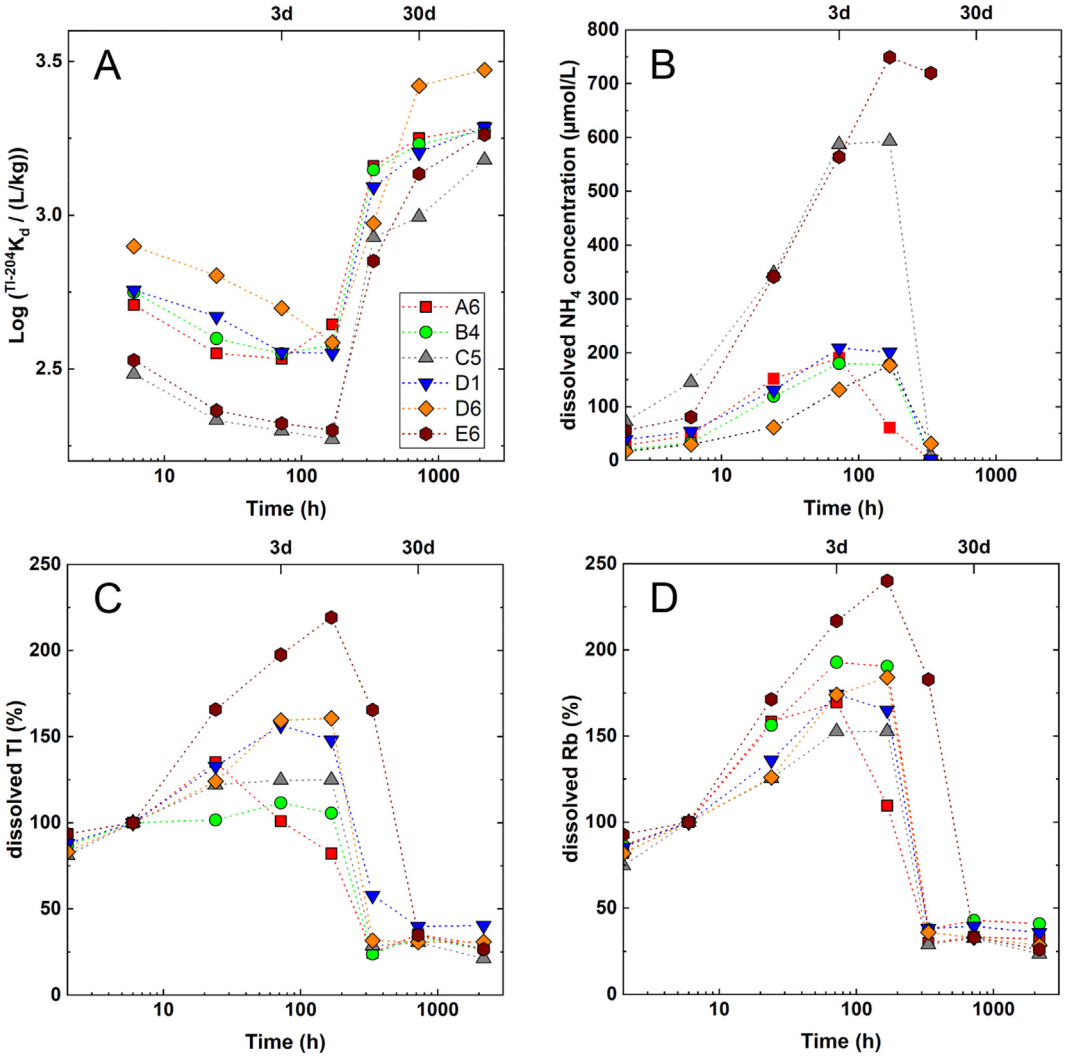

Fig. 2. (A) Log($^{Tl\text{-}204}K_d$/(L/kg)) from the kinetic isotope exchange experiment as a function of equilibration time. (B) Dissolved NH_4^+, (C) Tl, and (D) Rb in corresponding $CaCl_2$ equilibration experiments without radiotracer. In panels (C) and (D), concentrations are normalized to concentrations after 4 h of equilibration (plus 2 h pre-equilibration).

Table 2
Sequential extraction of exchangeable Tl and of reductively mobilizable Tl and Mn. Results for six selected soils and average and standard deviation (in parentheses) for all analyzed soils (n = 18). The complete results are listed in the Appendix.

Soil	Dissolved	Exchangeable	Reducible[a]				
	Tl_{CaCl2} (M)	Tl_{NH4} (%tot)	Tl (%tot)	Mn (%tot)	Tl/Mn (mol/mol)	Tl_{MnO2} (mol/kg)	Log $^{Tl}K_{d,MnO2}$ (L/kg)
A6	1.13×10^{-9}	2.6	2.2	83.4	1.89×10^{-5}	1.68×10^{-4}	5.2
B2	1.05×10^{-8}	4.8	2.3	70.6	3.78×10^{-5}	3.36×10^{-4}	4.5
C6	7.93×10^{-9}	1.4	0.5	55.1	1.74×10^{-4}	1.55×10^{-3}	5.3
D1	2.51×10^{-8}	4.0	1.6	77.5	2.99×10^{-4}	2.66×10^{-3}	5.0
E6	2.41×10^{-7}	5.6	2.9	67.3	3.74×10^{-3}	3.33×10^{-2}	5.1
F6	8.42×10^{-7}	5.2	1.3	45.0	4.78×10^{-3}	4.25×10^{-2}	4.7
Average[b]	–	3.7 (1.6)	2.0 (1.3)	58.0 (15.6)	–	–	5.2 (0.3)

[a] The Tl loading of Mn oxides (Tl_{MnO2}) is calculated from the molar Tl/Mn ratio in the reducible fraction, based on average Mn content of Mn oxide of 8.9 mol/kg (Wick et al., 2019), and the log K_d values for Tl sorption onto soil Mn oxides (log $^{Tl}K_{d,MnO2}$) are calculated from the Tl loading of Mn oxides and the dissolved Tl concentration in the $CaCl_2$ extract.

[b] Average (and standard deviation in parentheses) for all 18 soils analyzed by sequential extraction.

19 ± 8%, and K for 2 ± 1% of the sum of exchangeable charge equivalents.

A test with four consecutive 1 M NH_4-acetate extraction steps performed with six selected soil samples showed that 2.6 ± 0.9% of the total Tl was extracted in the first step, 1.1 ± 0.3% in the second step, 0.5 ± 0.2% in the third step and 0.3 ± 0.1%, in the fourth step (Table S6). This indicated that the two-step extraction use for all soils extracted ~83% of the exchangeable Tl.

3.3. Dissolved cations in the pseudo-porewater extracts

Dissolved concentrations of Tl in the $CaCl_2$ extracts of six selected soils as well as the average and range for all soils are listed in Table 1 (complete results given in Table S7). Dissolved Tl_{CaCl2} ranged from 0.1 to 270 µg/L and was closely correlated with total Tl (r = 0.97 for log-transformed data; Fig. 1B) and exchangeable Tl (r = 0.99 for log-transformed data; Fig. 1C).

Tests with six selected soils showed that over four sequential equilibrations in 0.01 M $CaCl_2$, dissolved Tl concentrations in the fourth equilibration corresponded to 47 ± 7% of the concentrations in the first equilibration (Table S8). This decrease most probably reflects a gradual depletion of the most readily equilibrating fraction of the exchangeable Tl pool. Alternatively, the decrease could be linked to decreasing concentrations of dissolved K over repeated $CaCl_2$ extractions and a resulting decrease in sorption competition between K and Tl for more specific cation exchange sites.

3.4. NH_4-exchangeable versus $CaCl_2$-dissolved Tl

In Fig. 1C, log-transformed exchangeable Tl_{NH4} contents are plotted against log-transformed dissolved Tl_{CaCl2} for all 36 soil samples. In a broad sense, this plot can be interpreted as a (de)sorption isotherm for exchangeable geogenic Tl. Linear regression of this pseudo-isotherm returned a slope close to unity ($y = 2.13 + 0.94x$; $R^2 = 0.96$). As shown in Fig. 1D, the same data can be plotted as distribution coefficients ($^{Tl}K_{d,geo}$; Eq. (1)) versus dissolved Tl. This plot indicates a small decrease in the log ($^{Tl}K_{d,geo}$/(L/kg)) over a nearly three orders of magnitude increase in Tl_{CaCl2} and total Tl. From all soils, an average $^{Tl}K_{d,geo}$ of 2.60 ± 0.20 is calculated.

$K_{d,geo}$ values for Rb, K, Ba, and Mg were calculated analogously to $^{Tl}K_{d,geo}$ (Table 9). Over the 36 soils, a close correlation was observed between the log K_d values of Tl and Rb (r = 0.82), K (r = 0.76) and Ba (r = 0.75), but only a low correlation with Mg (r = 0.35), indicating that exchangeable Tl strongly interacted with Rb as well as K and Ba, but hardly with Mg (Table S10).

3.5. Kinetic ^{204}Tl isotope exchange

The results of the isotope exchange experiments with six soils are displayed in Fig. 2 and listed in Table S11. On average, log ($^{Tl\text{-}204}K_d$/(L/kg)) values after 4 h equilibration with ^{204}Tl were 0.2 ± 0.1 higher than log ($^{Tl}K_{d,geo}$/(L/kg)) values derived from NH_4-acetate exchangeable and $CaCl_2$-soluble Tl. Accordingly, the pools of radiolabile Tl after 4 h equilibration were about 1.6 ± 0.4 times higher than the pools of exchangeable Tl determined by the two step 1 M NH_4-acetate extraction. This finding is partly in line with the observation that two extraction steps with 1 M NH_4-acetate extracted up to 20% less Tl than four steps. Furthermore, it is possible that the 1 M NH_4-acetate used in the extracts may have caused the partial collapse of the frayed edges of illite and the trapping of exchangeably adsorbed Tl, as has been suggested for Cs (de Koning and Comans, 2004).

Interestingly, NH_4 concentrations in the $CaCl_2$-extracts of all six soils rapidly increased over the first seven days of equilibration and decreased again thereafter, most probably due to microbial ammonification (N-mineralization) that liberates NH_4^+ (Blume et al., 2016). After 30 d of reaction, NH_4 concentrations in all soils were below 7 µmol/L. In parallel to these changes in dissolved NH_4^+ concentrations, the concentrations of Tl and Rb in solution markedly increased and decreased again, pointing to their release by highly specific sorption competition with NH_4^+, in line with Cs^+ mobilization from sediments due to ammonification (Comans et al., 1989; Evans et al., 1983). In addition, the close co-evolution of dissolved Tl and Rb concentrations during equilibration showed that the same type of adsorption process affected both cations.

The log $^{Tl\text{-}204}K_d$ values decreased with increasing NH_4^+ concentrations, before they increased again with disappearing dissolved NH_4^+. These coupled trends suggested that NH_4^+ temporarily also displaced initially adsorbed ^{204}Tl. The log $^{Tl\text{-}204}K_d$ values after 90-d equilibration were 0.6 ± 0.1 higher than after 4-h equilibration, indicating that ^{204}Tl at the end of the experiment had become more strongly sorbed than initially. The dissolved Tl concentrations in the $CaCl_2$-extracts after 90-d equilibration, on the other hand, were 69 ± 7% lower than after 4-h equilibration. Consequently, the pools of radiolabile Tl were on average only 1.2 ± 0.2 times higher after 90-d equilibration, suggesting that fixation processes were too slow to be clearly reflected after 90 d, possibly also because of the confounding impacts of the temporary increase in dissolved NH_4^+ concentrations, which appeared to result in an increase in ^{204}Tl sorption strength. Cs studies also revealed strong effects of NH_4^+ on sorption reversibility when concentrations exceed 10^{-4} M NH_4^+ (de Koning and Comans, 2004).

3.6. Sequential extraction of exchangeable Tl and reductively mobilizable Tl and Mn

From the sequential extraction of exchangeable Tl and reductively mobilizable Tl and Mn, the results for six of the 18 analysed soil samples and the averages over all analysed soil samples are given in Table 2, the complete data is given in Table S12. Both extractions were performed in three consecutive extraction steps. Decreasing concentrations of Tl over the three extracts with 1 M NH_4-acetate (pH 6.8) indicated that the exchangeable pool was depleted (Fig. S2). The first extraction with 1 M NH_4-acetate + 0.1 M $NH_3OH \times HCl$ (pH 6.1) resulted in

a clear increase in the extracted Tl fraction. Since the pH was not much lower than in the proceeding steps, the increase in extracted Tl was attributed to the reductant hydroxylamine. The decrease in the Tl content over the 3 extraction steps with hydroxylamine indicated that the respective pool got also depleted. On average, 58% of the total soil Mn were extracted by hydroxylamine at pH 6.1 (Table S12), but less than 1% of the total Fe. Therefore, and because the NH_4-acetate in the hydroxylamine extract minimized the re-adsorption of reductively released Tl(I), the hydroxylamine extract was considered to adequately represent (non-exchangeable) Tl associated with reducible Mn oxides.

Over the 18 analysed soils, the fraction of Tl associated with Mn oxides ($2.0 \pm 1.3\%$) corresponded to about 59% of the exchangeable Tl fraction ($3.7 \pm 1.6\%$). Taking also the reducible Mn into account, the molar Tl/Mn ratios in the hydroxylamine extract and the corresponding loading of Mn oxides could be calculated based on the assumption that all Tl and Mn in the reducible fraction were associated with Mn oxides. Furthermore, assuming that the Tl sorbed onto Mn oxides was in equilibrium with the porewater, and using the Tl concentrations in the pseudo-porewater extract, log-transformed distribution coefficients for the sorption of Tl onto soil Mn oxides (log ($^{Tl}K_{d,MnO2}$/(L/kg)) were calculated, which varied over a rather narrow range for the 18 analysed soils (5.2 ± 0.3).

3.7. Tl adsorption and re-extraction

In Fig. 3, the adsorption isotherms for six soils together with the results from the subsequent re-extraction with $CaCl_2$ (dissolved Tl) and with NH_4-acetate (exchangeable Tl) are shown. The analogous plots as log transformed distribution coefficients versus dissolved Tl are shown in Figure S3. The entire adsorption and re-extraction data, as well as the evolution of pH and Tl, Rb, K, Ba, Mg, and Ca in a blank sample are summarized in the Appendix (Table S13 and S14). In general, the isotherms derived from the NH_4-acetate and $CaCl_2$ extracts (in analogy to the isotherm for geogenic Tl in Fig. 1) fell onto the same line as the adsorption isotherms of freshly adsorbed Tl. This close match suggested that the two extracts adequately described the relationship between exchangeably adsorbed and dissolved Tl. However, on average, only $68 \pm 14\%$ of the freshly adsorbed Tl was re-extracted as NH_4-exchangeable

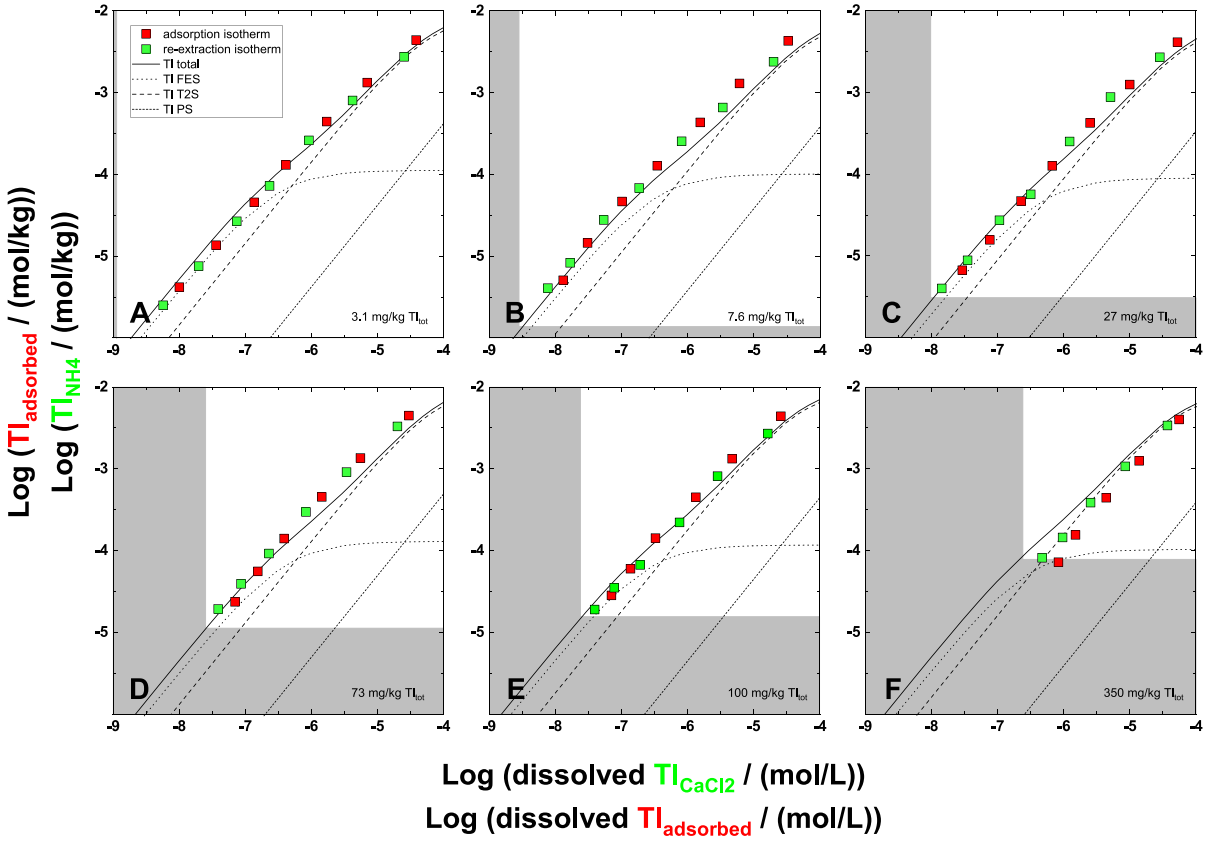

Fig. 3. Tl adsorption isotherms and corresponding exchangeable Tl contents (1 M NH_4-acetate) and dissolved Tl concentrations (0.01 M $CaCl_2$) for six soils ((A): A6; (B): B4; (C): C5; (D): D1; (E): D6; (F): E6) with geogenic Tl contents from ~4 to ~350 mg/kg, spiked with up to 1000 mg/kg Tl. Grey areas indicate the exchangeable contents and dissolved concentrations of geogenic Tl. Lines represent predictions based on the 3-site cation exchange model for Tl(I) adsorption onto illite (total, frayed edge sites (FES), type-2 sites (T2S) and planar sites (PS)), for cation concentrations in the individual pseudo-porewater extracts (Table S7) and scaled by the content of micaceous clay minerals (illite and musovite) in the individual soils (Table S2).

Tl, and dissolved Tl concentrations in the $CaCl_2$ extracts on average corresponded to 57 ± 5% of residual dissolved Tl in the adsorption experiments. These shifts suggested that part of the freshly adsorbed Tl had become fixed in less-exchangeable form (presumably in micaceous clay minerals), or that the NH_4-acetate and $CaCl_2$ extracts underestimated the respective quantities for methodological reasons.

3.8. Speciation of geogenic and adsorbed Tl by Tl L_{III}-edge XANES spectroscopy

In Fig. 4, the spectra of selected soil samples, of a soil clay mineral fraction, and of soils with freshly adsorbed Tl are compared to the four reference spectra selected for LCF analysis. A larger set of reference spectra (Fig. S4), the rationale for the selection of the four reference spectra shown in Fig. 4 for LCF analysis, LCF results (Table S15) and all sample spectra together with their LCF reconstructions (Fig. S5) are provided in the Appendix.

The overlay plot of three representative topsoil spectra with geogenic Tl contents of 10 mg/kg (B5), 102 mg/kg (D5), and 856 mg/kg (F5) reveals no marked spectral differences, indicating that Tl speciation was similar irrespective

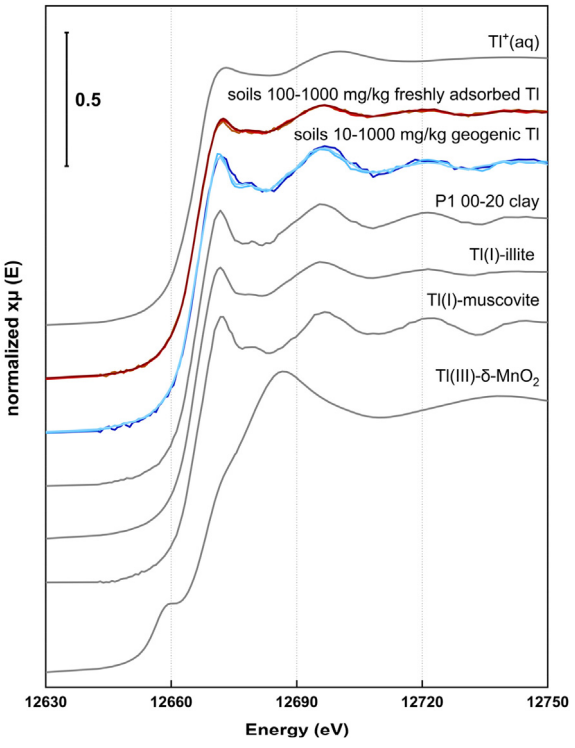

Fig. 4. Tl L_{III}-edge XANES spectra of soil samples with geogenic Tl loadings of 10 mg/kg (B5), 102 mg/kg (D5), and 856 mg/kg (F5), of geogenic Tl in a soil clay mineral fraction (P1 00-20 clay), and of soils (A6 and D1) with ~100–1000 mg/kg freshly sorbed Tl in comparison to four reference spectra (dehydrated Tl^+ adsorbed onto FES of illite (Tl(I)-illite) and in the interlayer of Ba-rich muscovite (Tl(I)-muscovite); Tl(III) sorbed onto δ-MnO_2 (Tl(III)-δ-MnO_2); hydrated aqueous Tl^+). See Appendix for further reference spectra and details on XAS data interpretation.

of total soil Tl contents. The LCF analysis (Table S15) of the soils with 7.6–1026 mg/kg geogenic Tl showed that Tl speciation was dominated (~98% on average) by Tl(I) associated with illite or other micaceous clay minerals. Remarkably, essentially the same spectrum was also recorded on a soil clay mineral fraction isolated from topsoil after the removal of soil organic matter and Fe and Mn oxides (P1 00-20 clay, Fig. 4), confirming the conclusion that Tl was associated with micaceous clay minerals. Because of the close similarity of the reference spectra Tl(I)-illite (Tl(I) adsorbed at the frayed edges of illite) and Tl(I)-muscovite (structural Tl(I) in the interlayer) (Fig. 4), however, XANES spectroscopy did not allow differentiating between Tl adsorption onto or structural incorporation into micaceous clay minerals.

The LCF analysis of some spectra pointed to a minor fraction of Tl(III). The fitted small Tl(III) fractions were associated with substantial uncertainty and could also have served to account for minor variations in energy calibration and instrumental resolution among spectra collected at different beamlines. On the other hand, if real, the small Tl(III) fractions were most probably associated with Mn oxides, noting that Tl(III) in Mn concretions has previously been identified in Erzmatt soils (Voegelin et al., 2015).

Avicennite (Tl_2O_3) and Tl(I)-jarosite have previously been identified as secondary minerals in mineralized Tl-rich subsoil horizons on the Erzmatt (Herrmann et al., 2018; Voegelin et al., 2015). Considering that the XANES spectrum of Tl(I)-jarosite is fairly distinctive (Fig. S4), the soil XANES spectra showed that this secondary mineral played a minor role in the topsoil samples, and that soil Tl speciation was dominated by pedogenic Tl species.

The overlay plot of the spectra of three soil samples with freshly adsorbed Tl at levels that exceed geogenic Tl contents by about ten to hundred times also closely matched each other. LCF analysis indicated that these spectra could be described by a major fraction of 65 ± 1% of Tl(I) associated with micaceous clay minerals (adsorbed or incorporated), a minor but uncertain fraction of Tl(III), as well as 27% ± 1% of hydrated Tl^+. This latter fraction may account for (hydrated) Tl^+ associated with illite or other clay minerals at higher loadings (Wick et al., 2018), Tl^+ adsorbed to certain Mn oxides (Peacock and Moon, 2012; Wick et al., 2019), Fe oxides or organic matter (Fig. S4). Thus, the spectra confirmed that most freshly adsorbed Tl was retained by micaceous clay minerals, but also pointed to Tl sorption to other soil components or less specific Tl sorption onto clay minerals at higher Tl loadings.

3.9. Model calculations for Tl adsorption onto micaceous soil clay minerals

The relationship between NH_4-acetate exchangeable and dissolved Tl in $CaCl_2$ extracts over all 36 soils was interpreted as an isotherm for exchangeable geogenic Tl. In Fig. 1C, this isotherm is compared to a prediction for Tl (I) adsorption onto micaceous soil clay minerals calculated with the 3-site cation exchange model for Tl, Rb, K, NH_4, Na, Mg and Ca adsorption onto illite (Wick et al., 2018). For this prediction, the average concentrations of Rb, K,

NH_4, Mg, and Ca in the $CaCl_2$ extracts of all 36 soils were used (Table S16) and only the Tl concentration was varied. Finally, the calculated exchanger composition was scaled to the average content of dioctahedral phyllosilicate (illite and muscovite) in the six soils examined by XRD ($16.8 \pm 2.0\%$). The predicted adsorption isotherm closely matched the relationship between exchangeable and dissolved Tl. Additional calculations based on the 5- and 95-percentile concentrations of competing cations in the $CaCl_2$ extracts (Table S16) were calculated to visualize potential variations in adsorbed amounts as a result of adsorption competition. Additional predictions were calculated based on the effective concentrations of all cations in the $CaCl_2$ extract of each soil (Table S7), which resulted in a slight improvement in fit quality (Fig. S6).

In the model calculations, adsorbed Tl in most soils was primarily allocated to the FES. Thus, Tl in these soils was assumed to be primarily adsorbed at the frayed edges of micaceous clay minerals where Tl^+ adsorption is mainly affected by adsorption competition with K^+ and NH_4^+. Although Rb^+ sorbs more strongly onto FES than K^+ or NH_4^+ (Wick et al., 2018) competition with Rb^+ was not relevant in the model calculations because of the low soil Rb concentrations relative to K and NH_4. In the soils with the highest geogenic Tl contents, the T2S contributed most to the modelled adsorbed Tl. From the experimental distributions coefficients of Tl, Rb and K, overall cation exchange selectivity coefficients for Tl-Rb and Tl-K exchange in the bulk soil materials were derived (Eq. (2)). Remarkably, model predictions for the log-transformed Tl-K exchange coefficient (0.95 ± 0.10) closely matched experimental values (0.97 ± 0.14). On the other hand, the model underestimated the adsorption of Rb by about 0.5 log units. By adjusting the cation exchange coefficient for Rb-Na exchange on FES in the model, the fits of sorbed Rb could be improved without affecting the model outcome for Tl^+, reflecting that Tl^+ adsorption is mainly affected by adsorption competition with K^+ and NH_4^+, rather than competition with the trace metal Rb^+.

The model predictions for Tl adsorption in the six soils used for the adsorption / re-extraction experiments also closely matched experimental adsorption as well as re-extraction data (Fig. 3 and S3). The highest dissolved Tl concentrations and exchangeably adsorbed Tl contents in the Tl-spiked soils were up to two orders of magnitude higher than the highest levels of geogenic Tl. For these highest Tl spike levels, the model calculations attributed most adsorbed Tl to the T2S as the FES were already saturated with Tl at lower dissolved Tl concentrations.

3.10. Tl adsorption onto Mn/Fe-enriched and Mn/Fe-depleted acidic soil material

Tl adsorption experiments with Mn/Fe-enriched and Mn/Fe-depleted soil material from the Sd horizon of an acidic pseudogley soil showed similar extents of Tl adsorption for both materials, i.e., no detectable effect of Mn oxides on Tl adsorption. Also the Tl L_{III}-edge XANES spectra provided no evidence for Tl association with Mn oxides, but indicated that essentially all Tl was retained by adsorption onto micaceous clay minerals, with illite and muscovite together accounting for ~11% of the soil mass (see section 11 in Appendix for further details).

4. DISCUSSION

The combined interpretation of all experimental results provides new insights into the importance of micaceous clay minerals for long-term Tl fixation and for short-term Tl adsorption via cation exchange in soils, as well as into the relevance of Mn oxides and other soil sorbent phases for Tl retention. These aspects and their environmental relevance are discussed in detail in this discussion section.

4.1. Fixation of Tl in the interlayers of micaceous clay minerals

The characterisation of the geogenic Tl by XAS indicated that nearly all soil Tl was associated with micaceous clay minerals. On the other hand, less than 10% of the total soil Tl was exchangeable with NH_4^+ or in isotope exchange with ^{204}Tl over up to 90 days reaction time. Accordingly, 90% or more of the total soil Tl most probably were fixed in the interlayers of micaceous clay minerals. This finding supports earlier studies on naturally Tl-enriched soils, in which high residual Tl fractions in sequential extractions or the correlation of Tl concentrations with soil clay content were attributed to the association of Tl with primary silicates including mica, or secondary illite (Tremel et al., 1997b; Vaněk et al., 2009). Considering that the Erzmatt soils developed on mineralized carbonate rock, and that hydrothermal muscovite can form as accessory mineral in hydrothermal brines (Heinrich and Candela, 2014; Runyon et al., 2019), hydrothermal Tl-enriched muscovite could have been a source of Tl-bearing clay minerals in the Erzmatt soils. However, total soil Tl tightly correlated with As, pointing to their co-release from hydrothermal pyrite. Furthermore, hydrothermal waters assumed to be analogous to the waters that led to Tl-As-Fe mineralization on the Erzmatt have temperatures below 100 °C and contain elevated concentrations of Rb in addition to Tl (Loges et al., 2012). Much higher temperatures, however, are required for the formation of hydrothermal muscovite, and the accumulation of Rb and Tl in hydrothermal muscovite would be expected to result in a tight correlation between total Tl and Rb contents in the Erzmatt soils. Consequently, we postulate that the fixation of Tl in micaceous minerals in topsoils on the Erzmatt occurred upon the release of Tl from weathering primary and secondary Tl-bearing minerals over the course of soil formation.

In the case of freshly adsorbed Tl, exchangeable contents and soluble concentrations of Tl determined after adsorption point to the potential fixation of a fraction of the freshly added Tl, in line with studies on the kinetics of Cs adsorption onto and desorption from illite (Comans, 1999; de Koning and Comans, 2004; Durrant et al., 2017). Importantly, although it has been shown that Cs gets fixed in illite over periods of weeks to months, desorption data indicate that fixed Cs should not be considered permanently immobilized, but that it may be slowly

released again over timescales of years to decades (Comans, 1999; Fuller et al., 2015). Similarly, Tl bound in the interlayers of phyllosilicates in soils from the Erzmatt may not be exchangeable over time scales relevant for soil cultivation and plant growth, but may be leached over longer time periods. Indeed, the observation that the fraction of exchangeable Tl does not vary greatly over nearly three orders of magnitude in total Tl in the Erzmatt soils possibly points to a (slow) equilibration between fixed and rapidly exchangeable Tl. The persistent high Tl levels in topsoils from the Erzmatt, on the other hand, indicate that Tl fixation in micaceous clay minerals substantially reduces Tl leaching, in line with the accumulation of Cs and Rb in weathered micaceous minerals observed in soils formed over thousands of years (Zaunbrecher et al., 2015b).

4.2. Adsorption of geogenic and spiked Tl onto micaceous clay minerals

Exchangeable geogenic Tl accounted for only 3.6 ± 1.6% of the total soil Tl contents, and could therefore not be characterized by bulk XAS. The XAS analysis of soils containing mainly freshly adsorbed Tl, however, showed that most of the added Tl adsorbed onto micaceous clay minerals (Fig. 4). For geogenic and freshly adsorbed Tl, the same relationship between NH_4-acetate-exchangeable Tl and dissolved Tl in pseudo-porewater extracts was observed, and this relationship matched the adsorption isotherms of the six soils (Fig. 5A). Furthermore, model predictions based on the cation exchange model for illite (Wick et al., 2018), on dissolved cation

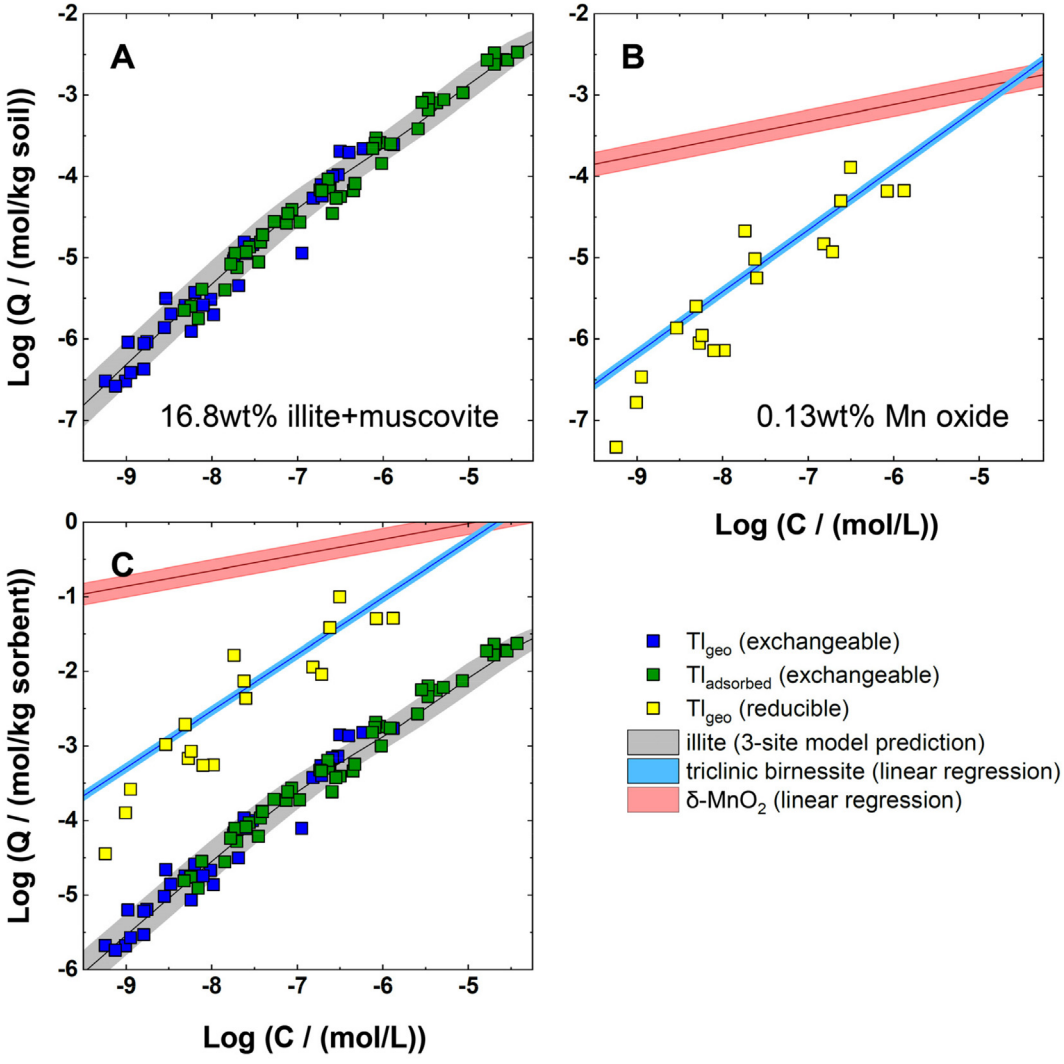

Fig. 5. (A) Comparison of pseudo-isotherms for exchangeable geogenic and freshly adsorbed Tl in Erzmatt soils with model predictions for Tl adsorption onto micaceous clay minerals in Erzmatt soil based on cation exchange model for illite (Wick et al., 2018) and porewater composition from $CaCl_2$ extracts (line; average cation concentrations grey area: 5- to 95-percentile cation concentrations). (B) Comparison of pseudo-isotherm for Tl associated with Mn oxides in Erzmatt soils to isotherms for oxidative Tl sorption onto δ-MnO_2 and nonoxidative Tl sorption onto triclinic birnessite (Wick et al., 2019) scaled by the average reducible Mn oxide content of the soils. (C) Same data as in panels (A) and (B), but with amounts of Tl over individual sorbent mass to visualize differences in sorption affinities.

concentrations in pseudo-porewater extracts, and on the content of micaceous clay minerals correctly predicted the amounts of exchangeable geogenic and freshly adsorbed Tl (Figs. 1, 3, and 5). In combination, the macroscopic Tl extraction and adsorption data, spectroscopic and modelling results unequivocally show that micaceous clay minerals determine the solubility of Tl in the studied soils, and that this sorption process can be described with the cation exchange model for illite (Wick et al., 2018). This finding is independently underpinned by the close correlations between geogenic Tl and Rb distribution coefficients derived from soil extractions and by the co-variation of dissolved Tl and Rb concentrations in response to changing NH_4^+ concentrations in the time-resolved $CaCl_2$ extractions (Fig. 2).

In the model calculations, geogenic Tl and Rb were nearly exclusively associated with the FES, and T2S became only relevant for freshly adsorbed Tl at the highest spike levels, where the FES were saturated with Tl. At lower and more common soil Tl concentrations, on the other hand, the FES were mainly saturated with K (~2/3) and NH_4 (~1/3). Changes in the concentration of these cations may therefore strongly affect Tl solubility, as has been shown in the past for Cs (Comans et al., 1989; de Koning and Comans, 2004; Evans et al., 1983). Ca and Mg, which mainly sorb onto the planar sites of micaceous clay minerals, on the other hand, may indirectly influence Tl solubility by displacing K and NH_4 from PS, thereby enhancing their competition with Tl for sorption onto T2S and especially FES.

The LCF analysis of the XANES spectra of freshly adsorbed Tl returned about 27% hydrated Tl. This hydrated Tl could represent less specifically adsorbed Tl on clay minerals, or hydrated Tl^+ adsorbed onto Mn oxides (Wick et al., 2019), Fe oxides (Casiot et al., 2011; Coup and Swedlund, 2015), or soil organic matter (Liu et al., 2011). Since freshly spiked and geogenic Tl exhibited the same relationship between exchangeable and dissolved Tl (Fig. 4), we speculate that the exchangeable geogenic Tl pool ($3.6 \pm 1.6\%$ of the total geogenic Tl) may include a similar percentage of hydrated Tl (27%). This fraction of less specifically adsorbed exchangeable Tl would thus correspond to $\sim 1.0 \pm 0.4\%$ of total geogenic soil Tl.

4.3. Sorption of Tl onto soil Mn oxides

Using micro-focused X-ray fluorescence spectrometry (μ-XRF), elevated concentrations of Tl in Mn-concretions in topsoil samples from the Erzmatt have previously been documented, and Tl in one concretion was identified as Tl(III) sorbed onto birnessite by μ-XANES and extended X-ray absorption fine structure (EXAFS) spectroscopy (Voegelin et al., 2015). Bulk XANES data collected in the present study (Fig. 4) did not allow to quantify the fractions of Tl(I) or Tl(III) associated with Mn oxides because the spectra were dominated by the large fraction of Tl associated with micaceous clay minerals.

The chemical fractionation of Tl in 18 soils by sequential extraction, however, returned Mn oxide-associated Tl fractions that were about half as high as the exchangeable fractions (Table S12). Thus, the fraction of Tl associated with Mn oxides via strong sorption can be of similar magnitude as the fraction associated with micaceous clay minerals via fast cation exchange, as reflected in the similarity of the pseudo-isotherms for exchangeable and Mn oxide associated Tl in the Erzmatt soils expressed in terms of sorbed Tl per soil mass (Fig. 5AB). This interpretation is in agreement with studies showing that freshly adsorbed Tl in soils is mostly associated with the "exchangeable" or "reducible" fractions (Lehn and Schoer, 1987; Vaněk et al., 2010a; Vaněk et al., 2010b; Vaněk et al., 2011), the latter fraction often being assumed to represent Tl sorbed onto Mn oxides.

From the sequential extraction data, the Tl loading of Mn oxides in the soils was estimated (Tables 2 and S12). These loadings (expressed per sorbent mass) were much higher than the amounts of exchangeable Tl associated with micaceous clay minerals (Fig. 5C), reflecting the fact that Mn oxides exhibit a higher affinity for Tl sorption than illite (Wick et al., 2019). The log K_d values derived from the chemical extraction data closely matched with log K_d values for nonoxidative Tl sorption onto triclinic birnessite or todorokite, but were much lower than log K_d values for oxidative Tl scavenging by δ-MnO_2 (Fig. 5BC). This observation seems to be in conflict with the earlier identification of Tl(III) in a Mn concretion in an Erzmatt soil (Voegelin et al., 2015). However, it is possible that only a minor fraction of the Mn oxides in the Erzmatt soils can sorb Tl oxidatively, or that natural birnessites in the studied soils have a much lower content of uncapped vacancy sites than freshly synthesized δ-MnO_2. Additional experiments with Mn/Fe-enriched and -depleted soil materials from an acidic pseudogley soil showed that Tl mainly adsorbed onto micaceous clay minerals, and provided no evidence for substantial Tl sorption onto Mn oxides. In combination, these results suggest that highly specific oxidative Tl uptake by soil Mn oxides may often be limited, possibly because (freshly formed) reactive Mn oxides rapidly transform into less reactive Mn oxides that cannot bind Tl oxidatively (Wick et al., 2019). Oxidative Tl uptake may therefore be limited to the timeframe of biological or autocatalytic Mn oxide formation in redox-dynamic soils, but less relevant for aged Mn oxides in soils.

4.4. Adsorption of Tl onto Fe oxides and soil organic matter

Fe oxides and soil organic matter can be alternative sorbents for Tl in soils (Casiot et al., 2011; Coup and Swedlund, 2015; Jacobson et al., 2005b; Liu et al., 2011; Martin et al., 2020; Vaněk et al., 2009). Quantitative estimates for the adsorption of Tl onto these sorbents were based on published adsorption isotherms recorded in Na or K electrolytes, and on estimates for the amounts of ferrihydrite and humic acid in the Erzmatt topsoils (Table S21). The estimated amounts of Tl adsorbed onto Fe oxides correspond to only $6 \pm 4\%$ of the NH_4-exchangeable geogenic Tl pool, the estimated amounts of Tl complexed by humic acids to only $11 \pm 7\%$. These estimates roughly match with the interpretation of the XANES data, which suggested that about 27% of the exchangeable geogenic Tl may be hydrated Tl,

which we assume to include Tl sorbed onto Fe oxides and organic matter (Section 4.2). However, the estimates of the amounts of Tl adsorbed onto Fe oxides or complexed by organic matter most probably represent upper limits, because sorption competition with major bivalent or trace metal cations and lower soil pH values than pH values in the sorption experiments were not taken into consideration. The estimates thus confirm the conclusion that exchangeable geogenic Tl in topsoils from the Erzmatt was mainly adsorbed onto micaceous clay minerals.

Although studies on the sorption of Tl onto ferrihydrite and humic acid have indicated that Tl^+ sorbs with a relatively low affinity comparable to K^+ (Coup and Swedlund, 2015; Martin et al., 2020), Fe oxides and organic matter may still be relevant sorbents for Tl under certain conditions. For example, adsorption of Tl onto organic matter may be important in organic-rich soil horizons or peats, as previously inferred from chemical extraction results (Vaněk et al., 2009), and in line with findings for Cs sorption to soils (Delvaux et al., 2001; Valcke and Cremers, 1994). Indeed, in a recent study on two soil profiles from the Erzmatt, elevated fractions of exchangeable Tl were observed in organic surface horizons and were accompanied by increased fractions of hydrated Tl^+ in the LCF analysis of corresponding XANES spectra (Vaněk et al., 2020), indicating that high levels of organic matter can sorb significant amounts of Tl in readily exchangeable form.

4.5. Environmental implications

This study showed that illite and other micaceous clay minerals play a key role in controlling the solubility of Tl in (contaminated) soils. In the long term, micaceous clay minerals can effectively sequester Tl by fixation in their interlayers. At the same time, micaceous clay minerals are important as sorbents of exchangeable Tl. The model developed for Tl adsorption onto illite (Wick et al., 2018) can be used to quantify the fast and reversible adsorption of Tl onto micaceous clay minerals in soils. The currently available data suggest that Tl in soils and sediments reacts largely in analogy to Cs and Rb (Wick et al., 2018). Accordingly, concepts developed to describe the reversible and irreversible sorption of Cs on illite (Brouwer et al., 1983; Comans, 1999; Comans et al., 1991; de Koning and Comans, 2004; Fuller et al., 2015) are transferable to Tl, but should be validated experimentally. Other clay minerals such as weathered biotite or vermiculite that have been shown to be important sorbents for Cs in other types of soils (Delvaux et al., 2001; Nakao et al., 2008; Valcke and Cremers, 1994; Zachara et al., 2002; Zaunbrecher et al., 2015a; Zaunbrecher et al., 2015b) can be expected to also strongly sorb Tl, with adsorption affinities intermediate between Cs and Rb.

The solubility of Tl adsorbed onto FES is strongly dependent on the dynamics of the main competing cations K^+ and NH_4^+. Therefore, agricultural practices that affect the concentrations of these cations, such as inorganic fertilizer or manure application, may have marked effects on the leaching and possibly also the plant uptake of Tl, although the latter also depends on the effects of K on Tl uptake into plants, as has been shown for Tl^+ uptake by algae (Hassler et al., 2007), and in analogy to the effects of K on the uptake of Cs by plants (Delvaux et al., 2000; Delvaux et al., 2001; Smolders et al., 1997). Also ammonification and denitrification processes and related changes in the NH_4^+ concentrations in the soil porewater may affect Tl adsorption onto FES in soils.

In the Erzmatt soils, Mn oxides play a minor role as sorbents for Tl. In anthropogenically Tl contaminated soils with a shorter contamination history, however, larger fractions of soil Tl could be associated with Mn oxides, as inferred from sequential extractions in earlier work (Antić-Mladenović et al., 2017; Gomez-Gonzalez et al., 2015; Vaněk et al., 2009; Vaněk et al., 2011; Yang et al., 2005). Owing to the much higher sorption affinity of oxidative Tl uptake by reactive Mn oxides than of cation exchange on micaceous clay minerals, oxidatively sorbed Tl may be less accessible through simple desorption. On the other hand, Tl associated with Mn oxides may become mobilized in waterlogged soil via reductive Mn oxide dissolution (and the reduction of poorly soluble Tl(III) into more soluble Tl(I)). Thus, Mn oxides can be highly effective sorbents for Tl, but with a limited chemical stability range. Furthermore, the highly selective sorption of a range of other trace metals onto Mn oxides (Grangeon et al., 2012; Manceau et al., 2002; Peacock and Sherman, 2007; Peña et al., 2015; Post, 1999; Simanova and Peña, 2015) may further limit their ability to sequester Tl, in contrast to micaceous clay minerals where K and NH_4 are the dominant competing cations in soils (Wick et al., 2018).

The present study provides a solid basis for a more quantitative and mechanistic understanding of Tl sorption processes in soils. In continuation of this work, aspects that warrant further consideration include: (i) the relevance of different Tl sorption processes over a wider range of soils with contrasting physicochemical characteristics (soil pH, organic C, Mn oxide and Fe oxide content, clay mineralogy), (iii) the kinetics of Tl adsorption and desorption processes in soils, (iii) consequences of reductive dissolution of Mn oxides, ammonification/denitrification, and sulfate reduction on the dynamics of dissolved Tl in periodically waterlogged soils, or (iv) the impact of soil fertilization with N and K on the solubility and soil-plant transfer of Tl in agricultural soils.

Declaration of Competing Interest

The authors declare that they have no known competing financial interests or personal relationships that could have appeared to influence the work reported in this paper.

ACKNOWLEDGEMENTS

Daniel Schmutz and Iwan Fankhauser (Amt für Umweltschutz und Energie, Kanton Basel-Landschaft, Switzerland) are kindly acknowledged for providing topsoil sample materials and data on acid-extractable element contents and soil pH, and Beda Hofmann (Natural History Museum, Berne, Switzerland) for providing Ba-rich muscovite (“oellacherite”) from Lengenbach. We thank Cornel

Niederhauser, Febin Ambalathattil, Irene Brunner, Marco Fleischmann (all Eawag) and Elmotaz Eltayeb (PSI) for their support in the laboratory. Prof. Dr. Christoph Heinrich (ETH Zürich) is acknowledged for insightful comments about the genesis of ore deposits. The Swiss Light Source (Paul Scherrer Institute (PSI), Villigen, Switzerland), the Dutch Belgian Beamline (DUBBLE; European Synchrotron Radiation Facility (ESRF), Grenoble, France), and the French National Synchrotron Soleil (Gif-sur-Yvette, France) are kindly acknowledged for the allocation of beam time, and Olga Safonova and Maarten Nachtegaal (SuperXAS, PSI), Dipanjan Banerjee (DUBBLE, ESRF), and Gautier Landrot (SAMBA, Soleil) for support during XAS data collection. This work was financially supported by the Swiss National Science Foundation under contract No. 200021-162364.

APPENDIX A. SUPPLEMENTARY MATERIAL

Supplementary data to this article can be found online at https://doi.org/10.1016/j.gca.2020.07.037.

REFERENCES

Adams A. and Diamond L. W. (2019) Facies and depositional environments of the Upper Muschelkalk (Schinznach Formation, Middle Triassic) in northern Switzerland. *Swiss J. Geosci.* **112**, 357–381.

Antić-Mladenović S., Frohne T., Kresović M., Stärk H. J., Savić D., Ličina V. and Rinklebe J. (2017) Redox-controlled release dynamics of thallium in periodically flooded arable soil. *Chemosphere* **178**, 268–276.

Bačeva K., Stafilov T., Šajn R., Tănăselia C. and Makreski P. (2014) Distribution of chemical elements in soils and stream sediments in the area of abandoned Sb-As-Tl Allchar mine, Republic of Macedonia. *Environ. Res.* **133**, 77–89.

Bergmann, J., Friedel, P. and Kleeberg, R. (1998) BGMN—a new fundamental parameters based Rietveld program for laboratory X-ray sources, its use in quantitative analysis and structure investigations. Commission of Powder Diffraction, International Union of Crystallography Newsletter 20.

Bergmann J. and Kleeberg R. (1998) Rietveld analysis of disordered layer silicates. *Mater. Sci. Forum* **278–281**, 300–305.

Blume H. P., Scheffer F. and Schachtschabel P. (2016) *Scheffer/Schachtschabel Soil Science*. Springer Verlag, Berlin, Heidelberg.

Bradbury M. H. and Baeyens B. (2000) A generalised sorption model for the concentration dependent uptake of caesium by argillaceous rocks. *J. Contam. Hydrol.* **42**, 141–163.

Brouwer E., Baeyens B., Maes A. and Cremers A. (1983) Cesium and rubidium ion equilibria in illite clay. *J. Phys. Chem.* **87**, 1213–1219.

Bunzl K., Trautmannsheimer M., Schramel P. and Reifenhäuser W. (2001) Availability of arsenic, copper, lead, thallium, and zinc to various vegetables grown in slag-contaminated soils. *J. Environ. Qual.* **30**, 934–939.

Casiot C., Egal M., Bruneel O., Verma N., Parmentier M. and Elbaz-Poulichet F. (2011) Predominance of aqueous Tl(I) species in the river system downstream from the abandoned Carnoules Mine (Southern France). *Environ. Sci. Technol.* **45**, 2056–2064.

Cheam V., Garbai G., Lechner J. and Rajkumar J. (2000) Local impacts of coal mines and power plants across Canada. I. Thallium in waters and sediments. *Water Qual. Res. J. Can.* **35**, 581–607.

Chen Y. H., Wang C. L., Liu J., Wang J., Qi J. Y. and Wu Y. J. (2013) Environmental exposure and flux of thallium by industrial activities utilizing thallium-bearing pyrite. *Sci. China-Earth Sci.* **56**, 1502–1509.

Comans R. N. J. (1999) Kinetics and reversibility of radiocesium sorption on illite and sediments containing illite, mineral-water interfacial reactions: kinetics and mechanisms. *Am. Chem. Soc.*, 179–201.

Comans R. N. J., Haller M. and DePreter P. (1991) Sorption of cesium on illite - Non-equilibrium behavior and reversibility. *Geochim. Cosmochim. Acta* **55**, 433–440.

Comans R. N. J., Middelburg J. J., Zonderhuis J., Woittiez J. R. W., De Lange G. J., Das H. A. and Van Der Weijden C. H. (1989) Mobilization of radiocesium in pore water of lake-sediments. *Nature* **339**, 367–369.

Coup K. M. and Swedlund P. J. (2015) Demystifying the interfacial aquatic geochemistry of thallium(I): New and old data reveal just a regular cation. *Chem. Geol.* **398**, 97–103.

Cremers A., Elsen A., DePreter P. and Maes A. (1988) Quantitative-analysis of radiocesium retention in soils. *Nature* **335**, 247–249.

Crittenden M. D., Cuttitta F., Rose H. J. and Fleischer M. (1962) Studies on manganese oxide minerals. 6. Thallium in some manganese oxides. *Am. Mineral.* **47**, 1461–1467.

Cruz-Hernández Y., Villalobos M., Marcus M. A., Pi-Puig T., Zanella R. and Martínez-Villegas N. (2019) Tl(I) sorption behavior on birnessite and its implications for mineral structural changes. *Geochim. Cosmochim. Acta* **248**, 356–369.

de Koning A. and Comans R. N. J. (2004) Reversibility of radiocaesium sorption on illite. *Geochim. Cosmochim. Acta* **68**, 2815–2823.

Delvaux B., Kruyts N. and Cremers A. (2000) Rhizospheric mobilization of radiocesium in soils. *Environ. Sci. Technol.* **34**, 1489–1493.

Delvaux B., Kruyts N., Maes E. and Smolders E. (2001) Fate of radiocesium in soil and rhizosphere. In *Trace Elements in the Rhizosphere* (eds. G. R. Gobran, W. W. Wenzel and E. Lombi), first ed. CRC Press LLC, Boca Raton, London, New York, Washington, D.C., pp. 61–91.

Döbelin N. and Kleeberg R. (2015) Profex: a graphical user interface for the Rietveld refinement program BGMN. *J. Appl. Crystallogr.* **48**, 1573–1580.

Durrant C. B., Begg J. D., Kersting A. B. and Zavarin M. (2017) Cesium sorption reversibility and kinetics on illite, montmorillonite, and kaolinite. *Sci. Total Environ.* **610–611**, 511–520.

Evans D. W., Alberts J. J. and Clark R. A. (1983) Reversible ion-exchange fixation of cesium-137 leading to mobilization from reservoir sediments. *Geochim. Cosmochim. Acta* **47**, 1041–1049.

Fuller A. J., Shaw S., Ward M. B., Haigh S. J., Mosselmans J. F. W., Peacock C. L., Stackhouse S., Dent A. J., Trivedi D. and Burke I. T. (2015) Caesium incorporation and retention in illite interlayers. *Appl. Clay Sci.* **108**, 128–134.

Gilkes, R.J. and McKenzie, R.M. (1988) Geochemistry and Mineralogy of Manganese in Soils, in: Graham, R.D., Hannam, R.J., Uren, N.C. (Eds.), Manganese in Soils and Plants: Proceedings of the International Symposium on 'Manganese in Soils and Plants' held at the Waite Agricultural Research Institute, The University of Adelaide, Glen Osmond, South Australia, August 22–26, 1988 as an Australian Bicentennial Event. Springer Netherlands, Dordrecht, pp. 23-35.

Gomez-Gonzalez M. A., Garcia-Guinea J., Laborda F. and Garrido F. (2015) Thallium occurrence and partitioning in soils and sediments affected by mining activities in Madrid province (Spain). *Sci. Total Environ.* **536**, 268–278.

Gonzalez R. (1990) Geometrie und Kinematik der Zeininger Bruch-Zone und eine Diskussion möglicher spätpaläozoischer Strukturen. *Eclogae Geol. Helv.* **83**, 513–523.

Grangeon S., Manceau A., Guilhermet J., Gaillot A. C., Lanson M. and Lanson B. (2012) Zn sorption modifies dynamically the layer and interlayer structure of vernadite. *Geochim. Cosmochim. Acta* **85**, 302–313.

Hassler C. S., Chafin R. D., Klinger M. B. and Twiss M. R. (2007) Application of the biotic ligand model to explain potassium interaction with thallium uptake and toxicity to plankton. *Environ. Toxicol. Chem.* **26**, 1139–1145.

Heinrich C. A. and Candela P. A. (2014) Fluids and Ore Formation in the Earth's Crust. In *Treatise on Geochemistry* (eds. H. D. Holland and K. K. Turekian), second ed. Elsevier, Oxford, pp. 1–28.

Heinrichs H., Schulz-Dobrick B. and Wedepohl K. H. (1980) Terrestrial geochemistry of Cd, Bi, Tl, Pb, Zn and Rb. *Geochim. Cosmochim. Acta* **44**, 1519–1533.

Herrmann J., Voegelin A., Palatinus L., Mangold S. and Majzlan J. (2018) Secondary Fe-As-Tl mineralization in soils near Buus in the Swiss Jura Mountains. *Eur. J. Mineral.* **30**, 887–898.

Houba V. J. G., Temminghoff E. J. M., Gaikhorst G. A. and van Vark W. (2000) Soil analysis procedures using 0.01 M calcium chloride as extraction reagent. *Commun. Soil Sci. Plant Anal.* **31**, 1299–1396.

Jackson M. (1968) Weathering of primary and secondary minerals in soils. *Int. Congr, Soil Sci., Trans. 9th (Adelaide, Australia)* **4**, 281–292.

Jacobson A. R., Klitzke S., McBride M. B., Baveye P. and Steenhuis T. S. (2005a) The desorption of silver and thallium from soils in the presence of a chelating resin with thiol functional groups. *Water, Air, Soil Pollut.* **160**, 41–54.

Jacobson A. R., McBride M. B., Baveye P. and Steenhuis T. S. (2005b) Environmental factors determining the trace-level sorption of silver and thallium to soils. *Sci. Total Environ.* **345**, 191–205.

Jović V. (1993) Thallium in rocks, soils and plants - past progress and future-needs. *Neues Jahrbuch für Mineralogie-Abhandlungen* **166**, 43–52.

Kabata-Pendias A. (2011) *Trace Elements in Soils and Plants*, fourth ed. CRC Press, Boca Raton.

Karbowska B. (2016) Presence of thallium in the environment: sources of contaminations, distribution and monitoring methods. *Environ. Monit. Assess.*, 188.

Kersten M., Xiao T., Kreissig K., Brett A., Coles B. J. and Rehkämper M. (2014) Tracing anthropogenic thallium in soil using stable isotope compositions. *Environ. Sci. Technol.* **48**, 9030–9036.

Koschinsky A. and Hein J. R. (2003) Uptake of elements from seawater by ferromanganese crusts: solid-phase associations and seawater speciation. *Mar. Geol.* **198**, 331–351.

LaCoste C., Robinson B. and Brooks R. (2001) Uptake of thallium by vegetables: Its significance for human health, phytoremediation, and phytomining. *J. Plant Nutr.* **24**, 1205–1215.

Lee J., Park S. M., Jeon E. K. and Baek K. (2017) Selective and irreversible adsorption mechanism of cesium on illite. *Appl. Geochem.* **85**, 188–193.

Lehn H. and Schoer J. (1987) Thallium-transfer from soils to plants - Correlation between chemical form and plant uptake. *Plant Soil* **97**, 253–265.

Liu J. A., Lippold H., Wang J., Lippmann-Pipke J. and Chen Y. H. (2011) Sorption of thallium(I) onto geological materials: Influence of pH and humic matter. *Chemosphere* **82**, 866–871.

Loges A., Wagner T., Kirnbauer T., Göb S., Bau M., Berner Z. and Markl G. (2012) Source and origin of active and fossil thermal spring systems, northern Upper Rhine Graben, Germany. *Appl. Geochem.* **27**, 1153–1169.

Lopez-Arce P., Garcia-Guinea J. and Garrido F. (2017) Chemistry and phase evolution during roasting of toxic thallium-bearing pyrite. *Chemosphere* **181**, 447–460.

Madejón P., Murillo J. M., Marañón T. and Lepp N. W. (2007) Factors affecting accumulation of thallium and other trace elements in two wild Brassicaceae spontaneously growing on soils contaminated by tailings dam waste. *Chemosphere* **67**, 20–28.

Makridis, C. and Amberger, A. (1996) Thallium concentration in soils and crops and critical values with respect to food chain, in: Rodriguez-Barrueco, C. (Ed.), Fertilizers and Environment: Proceedings of the International Symposium "Fertilizers and Environment", held in Salamanca, Spain, 26–29, September, 1994. Springer Netherlands, Dordrecht, pp. 443-448.

Manceau A., Lanson B. and Drits V. A. (2002) Structure of heavy metal sorbed birnessite. Part III: Results from powder and polarized extended X-ray absorption fine structure spectroscopy. *Geochim. Cosmochim. Acta* **66**, 2639–2663.

Marcus M. A., MacDowell A. A., Celestre R., Manceau A., Miller T., Padmore H. A. and Sublett R. E. (2004) Beamline 10.3.2 at ALS: a hard X-ray microprobe for environmental and materials sciences. *J. Synchrotron Radiat.* **11**, 239–247.

Martin L. A., Simonucci C., Rad S. and Benedetti M. F. (2020) Effect of natural organic matter on thallium and silver speciation. *J. Environ. Sci. (China)* **93**, 185–192.

Martin L. A., Wissocq A., Benedetti M. F. and Latrille C. (2018) Thallium (Tl) sorption onto illite and smectite: Implications for Tl mobility in the environment. *Geochim. Cosmochim. Acta* **230**, 1–16.

Matthews A. D. and Riley J. P. (1970) The occurrence of thallium in sea water and marine sediments. *Chem. Geol.* **6**, 149–152.

Meunier A. and Velde B. (2004) *Illite: Origins, Evolution and Metamorphism*. Springer-Verlag, Berlin, Heidelberg.

Nakao A., Thiry Y., Funakawa S. and Kosaki T. (2008) Characterization of the frayed edge site of micaceous minerals in soil clays influenced by different pedogenetic conditions in Japan and northern Thailand. *Soil Sci. Plant Nutr.* **54**, 479–489.

Nriagu J. O. (1998) *Thallium in the Environment*. John Wiley and Sons, New York, Chichester, Weinheim, Brisbane, Singapore, Toronto.

Omotoso O., McCarty D. K., Hillier S. and Kleeberg R. (2006) Some successful approaches to quantitative mineral analysis as revealed by the 3rd Reynolds Cup contest. *Clays Clay Miner.* **54**, 748–760.

Parkhurst D. L. and Appelo C. A. J. (1999) *User's Guide to PhreeqC (Version 2) - A Computer Program for Speciation, Batch-Reaction, One-dimensional Transport, and Inverse Geochemical Calculations*. U.S. Geological Survey, Denver, Colorado.

Peacock C. L. and Moon E. M. (2012) Oxidative scavenging of thallium by birnessite: Explanation for thallium enrichment and stable isotope fractionation in marine ferromanganese precipitates. *Geochim. Cosmochim. Acta* **84**, 297–313.

Peacock C. L. and Sherman D. M. (2007) Sorption of Ni by birnessite: Equilibrium controls on Ni in seawater. *Chem. Geol.* **238**, 94–106.

Peña J., Bargar J. R. and Sposito G. (2015) Copper sorption by the edge surfaces of synthetic birnessite nanoparticles. *Chem. Geol.* **396**, 196–207.

Peter A. L. and Viraraghavan T. (2005) Thallium: a review of public health and environmental concerns. *Environ. Int.* **31**, 493–501.

Pietsch J. S., Wetzel A. and Jordan P. (2016) A new lithostratigraphic scheme for the Schinznach Formation (upper part of the Muschelkalk Group of northern Switzerland). *Swiss J. Geosci.* **109**, 285–307.

Poinssot C., Baeyens B. and Bradbury M. H. (1999) Experimental and modelling studies of caesium sorption on illite. *Geochim. Cosmochim. Acta* **63**, 3217–3227.

Post J. E. (1999) Manganese oxide minerals: crystal structures and economic and environmental significance. *Proc. Natl. Acad. Sci. U.S.A.* **96**, 3447–3454.

Rader S. T., Maier R. M., Barton M. D. and Mazdab F. K. (2019) Uptake and fractionation of thallium by Brassica juncea in a geogenic thallium-amended substrate. *Environ. Sci. Technol.* **53**, 2441–2449.

Ravel B. and Newville M. (2005) ATHENA, ARTEMIS, HEPHAESTUS: data analysis for X-ray absorption spectroscopy using IFEFFIT. *J. Synchrotron Radiat.* **12**, 537–541.

Rehkämper M., Frank M., Hein J. R. and Halliday A. (2004) Cenozoic marine geochemistry of thallium deduced from isotopic studies of ferromanganese crusts and pelagic sediments. *Earth Planet. Sci. Lett.* **219**, 77–91.

Rehkämper M. and Nielsen S. G. (2004) The mass balance of dissolved thallium in the oceans. *Mar. Chem.* **85**, 125–139.

Runyon S. E., Seedorff E., Barton M. D., Steele-MacInnis M., Lecumberri-Sanchez P. and Mazdab F. K. (2019) Coarse muscovite veins and alteration in porphyry systems. *Ore Geol. Rev.* **113**, 1–32.

Sawhney B. L. (1972) Selective sorption and fixation of cations by clay-minerals - review. *Clays Clay Miner.* **20**, 93–100.

Schauer M. and Aigner T. (1997) Cycle stacking pattern, diagenesis and reservoir geology of peritidal dolostones, Trigonodus-dolomite, upper Muschelkalk (Middle Triassic, SW-Germany). *Facies* **37**, 99–113.

Shannon R. D. (1976) Revised effective ionic radii and systematic studies of interatomic distances in halides and chaleogenides. *Acta Crystallogr.* **A32**, 751–767.

Simanova A. A. and Peña J. (2015) Time-resolved investigation of cobalt oxidation by Mn(III)-rich δ-MnO2 using quick X-ray absorption spectroscopy. *Environ. Sci. Technol.* **49**, 10867–10876.

Smolders E., Van den Brande K. and Merckx R. (1997) Concentrations of Cs-137 and K in soil solution predict the plant availability of Cs-137 in soils. *Environ. Sci. Technol.* **31**, 3432–3438.

Tebo B. M., Bargar J. R., Clement B. G., Dick G. J., Murray K. J., Parker D., Verity R. and Webb S. M. (2004) Biogenic manganese oxides: Properties and mechanisms of formation. *Annu. Rev. Earth Planet. Sci.* **32**, 287–328.

Tremel A., Masson P., Garraud H., Donard O. F., Baize D. and Mench M. (1997a) Thallium in French agrosystems II. Concentration of thallium in field-grown rape and some other plant species. *Environ. Pollut.* **97**, 161–168.

Tremel A., Masson P., Sterckeman T., Baize D. and Mench M. (1997b) Thallium in French agrosystems I. Thallium contents in arable soils. *Environ. Pollut.* **95**, 293–302.

Truninger E. (1922) Arsen als natürliches Bodengift in einem Schweizerischen Kulturboden - Der Boden der Erzmatt bei Buus (Baselland). *Landwirtschaftliches Jahrbuch Schweiz* **36**, 1015–1030.

Valcke E. and Cremers A. (1994) Sorption-desorption dynamics of radiocesium in organic-matter soils. *Sci. Total Environ.* **157**, 275–283.

Vaněk A., Chrastný V., Komárek M., Galušková I., Drahota P., Grygar T., Tejnecký V. and Drábek O. (2010a) Thallium dynamics in contrasting light sandy soils - Soil vulnerability assessment to anthropogenic contamination. *J. Hazard. Mater.* **173**, 717–723.

Vaněk A., Chrastný V., Mihaljevič M., Drahota P., Grygar T. and Komárek M. (2009) Lithogenic thallium behavior in soils with different land use. *J. Geochem. Explor.* **102**, 7–12.

Vaněk A., Komárek M., Chrastný V., Bečka D., Mihaljevič M., Šebek O., Panušková G. and Schusterová Z. (2010b) Thallium uptake by white mustard (Sinapis alba L.) grown on moderately contaminated soils-Agro-environmental implications. *J. Hazard. Mater.* **182**, 303–308.

Vaněk A., Komárek M., Vokurková P., Mihaljevič M., Šebek O., Panušková G., Chrastný V. and Drábek O. (2011) Effect of illite and birnessite on thallium retention and bioavailability in contaminated soils. *J. Hazard. Mater.* **191**, 170–176.

Vaněk A., Voegelin A., Mihaljevič M., Ettler V., Trubač J., Drahota P., Vaňková M., Oborná V., Vejvodová K., Penížek V., Pavlů L., Drabek O., Vokurková P., Zádorová T. and Holubík O. (2020) Thallium stable isotope ratios in naturally Tl-rich soils. *Geoderma* **364**.

Voegelin A., Pfenninger N., Petrikis J., Majzlan J., Plötze M., Senn A. C., Mangold S., Steininger R. and Göttlicher J. (2015) Thallium speciation and extractability in a thallium- and arsenic-rich soil developed from mineralized carbonate rock. *Environ. Sci. Technol.* **49**, 5390–5398.

Wick S., Baeyens B., Marques Fernandes M. and Voegelin A. (2018) Thallium adsorption onto illite. *Environ. Sci. Technol.* **52**, 571–580.

Wick S., Peña J. and Voegelin A. (2019) Thallium sorption onto manganese oxides. *Environ. Sci. Technol.* **53**, 13168–13178.

Xiao T., Guha J., Boyle D., Liu C. Q. and Chen J. (2004) Environmental concerns related to high thallium levels in soils and thallium uptake by plants in southwest Guizhou, China. *Sci. Total Environ.* **318**, 223–244.

Xiao T., Yang F., Li S., Zheng B. and Ning Z. (2012) Thallium pollution in China: A geo-environmental perspective. *Sci. Total Environ.* **421–422**, 51–58.

Xiao T. F., Boyle D., Guha J., Rouleau A., Hong Y. T. and Zheng B. S. (2003) Groundwater-related thallium transfer processes and their impacts on the ecosystem: southwest Guizhou Province, China. *Appl. Geochem.* **18**, 675–691.

Yang C., Chen Y., Peng P., Li C., Chang X. and Xie C. (2005) Distribution of natural and anthropogenic thallium in the soils in an industrial pyrite slag disposing area. *Sci. Total Environ.* **341**, 159–172.

Zachara J. M., Smith S. C., Liu C. X., McKinley J. P., Serne R. J. and Gassman P. L. (2002) Sorption of Cs+ to micaceous subsurface sediments from the Hanford site, USA. *Geochim. Cosmochim. Acta* **66**, 193–211.

Zaunbrecher L. K., Cygan R. T. and Elliott W. C. (2015a) Molecular models of cesium and rubidium adsorption on weathered micaceous minerals. *J. Phys. Chem. A* **119**, 5691–5700.

Zaunbrecher L. K., Elliott W. C., Wampler J. M., Perdrial N. and Kaplan D. I. (2015b) Enrichment of cesium and rubidium in weathered micaceous materials at the Savannah River Site, South Carolina. *Environ. Sci. Technol.* **49**, 4226–4234.

Zeien H. and Brümmer G. W. (1989) Chemische Extraktionen zur Bestimmung von Schwermetallbildungformen in Boden. *Mitteilgn. Dtsch. Bodenkundl. Gesellsch.* **59**, 505–510.

Zitko V. (1975) Toxicity and pollution potential of thallium. *Sci. Total Environ.* **4**, 185–192.

Associate editor: Caroline L. Peacock